Monthly Notices of the ROYAL ASTRONOMICAL SOCIETY

MNRAS **547,** 1–17 (2026) https://doi.org/10.1093/mnras/stag434
Advance Access publication 2026 March 6

# Comprehensive insights into organic matter from astrophysical ice analogues by multimodal ionization high-resolution mass spectrometry

Lawry Honold,[1] Jasmine Hertzog,[2] Alexander Ruf,[3,4] Frédéric Aubriet,[2] Vincent Carré,[2] Philippe Schmitt-Kopplin,[5,6] Alicja Domaracka[7] and Grégoire Danger[1,8]*

[1]*Aix-Marseille Université, PIIM (Physics of the Interactions of Ions and Molecules), UMR 7345, CNRS, F-13013 Marseille, France*
[2]*Université de Lorraine, LCP–A2MC (Laboratoire de Chimie et Physique-Approche Multi-échelles des Milieux Complexes), F-57000 Metz, France*
[3]*Faculty of Physics, LMU Munich, Schellingstr 4, D-80799 Munich, Germany*
[4]*The Ludwigs-Maximillians-Universität (LMU), the Technical University of Munich (TUM), Excellence Cluster ORIGINS, Boltzmannstr 2, D-85748 Garching, Germany*
[5]*Research Unit Analytical BioGeoChemistry, Helmholtz-Zentrum Muenchen-German Research Center for Environmental Health, Neuherberg, D-85764Germany*
[6]*Technishe Universität München, Chair of Analytical Food Chemistry, Freising -Weihenstephan, D-85354Germany*
[7]*Normandie University, ENSICAEN, UNICAEN, CEA, CNRS, CIMAP, F-14000 Caen, France*
[8]*Institut Universitaire de France (IUF), Paris, F-75000France*

Accepted 2026 February 25. Received 2026 February 19; in original form 2025 December 8

## ABSTRACT

Advancing the limits of molecular characterization is essential in astrochemistry to elucidate the mechanisms involved in the formation and evolution of organic matter during the early stages of the Solar system. In this work, we employed a multimodal ionization approach to extend the description of the organic diversity present in residues formed during the VUV (Vacuum Ultra Violet) processing of interstellar ices analogues composed of $H_2O$-$CH_3OH$-$NH_3$ mixtures. The soluble organic fraction was extracted with methanol and analysed with high-resolution FT-ICR (Fourier-transform ion cyclotron resonance mass spectrometry), using electrospray ionization (ESI) and atmospheric pressure photoionization (APPI), both in positive and negative modes. About 15 000 distinct molecular formulas were detected, enhancing the characterization of such samples from a factor of three. While ESI offered the most comprehensive molecular coverage, detecting CHO, CHN, and CHNO species, APPI in positive mode revealed additional, previously undetected compounds. These newly observed assignments were mainly heteroatom-poor and unsaturated molecules, including low-oxidized and aromatic CHO structures, as well as CHN molecular formulas consistent with N-heterocyclic features. In contrast, APPI (−) proved to be limited for characterizing these samples. On average, the residue exhibits typical characteristics: H/C = 1.68; O/C = 0.33; N/C = 0.31; *m/z* 419.76046; formula = $C_{19}H_{31}N_5O_5$; double bond equivalent (DBE) = 7; and aromaticity equivalent ($X_c$) = 1.93. Present multimodal ionization approach provides new insights into the chemical diversity of soluble organic matter analogues and highlights the complementary strengths and limitations of each ionization mode, thereby contributing to enhance our understanding of the organic diversity observed in astrophysical environments.

**Key words:** astrobiology – astrochemistry – molecular processes – methods: analytical – methods: laboratory: molecular – ISM: molecules.

## 1. INTRODUCTION

Understanding the formation and evolution of organic compounds present within hot molecular cores is crucial to determine the origins of a fraction of the chemical diversity observed in interplanetary objects. Current observations of astrophysical objects leading to planetary systems allow the detection of the most abundant molecules in these environments, primarily through gas-phase measurements (A. C. A. Boogert, P. A. Gerakines & D. C. B. Whittet 2015; A. C. A. Boogert et al., 2022; see the Koeln database for Molecules in Space, available at: https://cdms.astro.uni-koeln.de/classic/molecules; C. P. Endres et al., 2016). Recent studies, notably taking advantage of the high sensitivity of the *James Webb Space Telescope*, have also been able to detect the most abundant chemical species in ices present in star-forming regions (M. K. McClure et al., 2023; W. R. M. Rocha et al., 2024). However, such observations provide only limited insights into the potential molecular diversity that may arise during the evolution

* E-mail: gregoire.danger@univ-amu.fr

of interstellar ices from dense molecular clouds to planetary system.

Analyses of pristine material from the interplanetary medium allow us to probe the potential organic matter that may have formed in such environments, and to assess how it may subsequently evolve in different objects within the inner or outer Solar system. Over the past decades, advanced analytical chemistry techniques have been applied to multiple extraterrestrial samples, including returned samples from asteroids (J. C. Aponte et al. 2023; H. Naraoka et al. 2023; P. Schmitt-Kopplin et al. 2023; Y. Furukawa et al. 2025; D. P. Glavin et al. 2025; A. Mojarro et al. 2025) and meteorites (P. Schmitt-Kopplin et al. 2010; N. Hertkorn, M. Harir & Ph. Schmitt-Kopplin 2015; J. Hertzog, H. Naraoka & P. Schmitt-Kopplin 2019; Y. Oba et al. 2020). These studies have enabled detailed characterization of these valuable samples and improved our understanding of the chemical evolution of organic matter within interplanetary objects.

Notably, an untargeted analytical technique, the high-resolution mass spectrometry (HRMS), such as FT-ICR MS (Fourier-transform ion cyclotron resonance mass spectrometry), provides rapid assessments of the global heteroatom composition in complex organic matrices without prior separation (A. G. Marshall, C. L. Hendrickson & G. S. Jackson 1998; E. N. Nikolaev, Y. I. Kostyukevich & G. N. Vladimirov 2016), and has been increasingly applied to these samples. Owing to their exceptional mass resolution and sensitivity, these analytical systems have led to the detection of thousands of distinct molecular species, greatly enhancing our understanding of the molecular diversity of organic matter formed in extraterrestrial environments and establishing them as indispensable tools in astrochemistry. Meteorites and returned samples thus offer valuable insights into the transformation of organic molecules (P. Schmitt-Kopplin et al. 2010; N. Hertkorn et al. 2015; A. Ruf et al. 2017; J. Hertzog et al. 2019; Y. Oba et al. 2020; J. C. Aponte et al. 2023; Y. Furukawa et al. 2025) and the physicochemical histories within observable bodies (J. C. Aponte et al. 2023; H. Naraoka et al. 2023; P. Schmitt-Kopplin et al. 2023; D. P. Glavin et al. 2025; A. N. Nguyen et al. 2025; S. A. Sandford et al. 2025). However, comparing them with pristine organic matter is essential to constrain potential scenario that could lead to organic matter observed in these natural objects (M. Bizzarro et al. 2025; D. P. Glavin et al. 2025; A. Mojarro et al. 2025).

In this context, laboratory astrophysics offers a complementary approach by developing experiments simulating the evolution of observed species, from dark molecular clouds up to protoplanetary discs, under various physicochemical constraints. Typically, representative interstellar ice analogues, composed of $H_2O$, $CH_3OH$, $NH_3$, CO, $CO_2$, $CH_4$, $N_2$, and/or $H_2S$ (H. M. Cuppen, H. Linnartz & S. Ioppolo 2024), are submitted to radiative processing that mimics the energetic conditions experienced by ices during the evolution of the solar nebula (Vacuum Ultra Violet / VUV photons, electrons, or ion bombardment; C. J. Shen et al. 2004; D. H. Wooden, S. B. Charnley & P. Ehrenfreund 2004; E. F. Van Dishoeck, B. Jonkheid & M. C. Van Hemert 2006; K. I. Öberg, 2016). These experiments are conducted in high/ultra-high vacuum conditions ($10^{-7}$ to $10^{-10}$ mbar) and at different temperatures (typically 10–77 K; V. K. Agarwal et al. 1985; R. Briggs et al. 1992; M. P. Bernstein et al. 1995; J. P. Dworkin et al. 2004; G. Danger et al. 2013; P. Modica et al. 2018; A. Bouquet et al. 2024), leading to the formation of organic residues when the sample is warmed up to room temperature. While targeted analyses of such residues have highlighted the ability of various chemical classes (e.g. carboxylic acids, aldehydes, amines, nitriles, amides, alcohols, and hydrocarbons) to form under interstellar ices conditions (V. K. Agarwal et al. 1985; R. Briggs et al. 1992; G. Strazzulla, A. C. Castorina & M. E. Palumbo 1995; Y. Takano et al. 2004; U. J. Meierhenrich et al. 2005; G. Danger et al. 2011; R. Hodyss et al. 2011; P. De Marcellus et al. 2015; C. Meinert et al. 2016; R. G. Urso et al. 2022; H. Naraoka et al. 2023), and among them, amino acids (M. P. Bernstein et al. 2002; Y. Takano et al. 2004; J. E. Elsila et al. 2007; M. Nuevo et al. 2007; P. De Marcellus et al. 2011; P. Modica et al. 2014, 2018; Y. Oba et al. 2019; A. Garcia et al. 2023, 2024; H. Naraoka et al. 2023), sugars (C. Meinert et al. 2016; M. Nuevo, G. Cooper & S. A. Sandford 2018), or nucleobases (Y. Oba et al. 2019; A. Ruf et al. 2019), as for natural objects, untargeted analyses with HRMS explores the potential molecular diversity present, from soluble to insoluble residue fractions, named soluble organic matter analogue (SOMA) or insoluble organic matter analogue (IOMA; G. Danger et al. 2022), respectively, providing a global view of their chemical evolution (M. P. Bernstein et al. 1995; G. M. Muñoz Caro & W. A Schutte 2003; P. Schmitt-Kopplin et al. 2010, 2023; G. Danger et al. 2013, 2021, 2022; C. K. Materese et al. 2015; N. Hertkorn et al. 2015; N. Abou Mrad et al. 2016; J. Hertzog et al. 2019; L. I. Tenelanda-Osorio et al. 2022; H. Naraoka et al. 2023; D. P. Glavin et al. 2025). HRMS analyses of residues, predominantly performed using electrospray ionization (ESI; P. Kebarle & L. Tang 1993; T. C. Rohner, N. Lion & H. H. Girault 2004; M. Wilm 2011), have thus demonstrated their remarkable molecular diversity (G. Danger et al. 2016, 2021, 2022; A. Ruf & G. Danger 2022), containing thousands of molecular formulas, with molecular masses reaching up to 4000 Da (G. Danger et al. 2013). These results can subsequently be compared to extraterrestrial samples analyses. Comparisons between Murchison meteorite analysed by FT-ICR MS and laboratory simulations of aqueous alteration, processes that may occur within interplanetary objects, performed on a SOMA, suggest that it may be possible to tend toward the organic content observed in certain interplanetary objects (G. Danger et al. 2021).

However, the detection of organic compounds strongly depends on the analytical methodology, and in particular, on the ionization technique employed, which can introduce significant biases and ultimately limit the chemical information obtained, specifically in the presence of high molecular diversities. Previous studies of both terrestrial (N. Hertkorn et al. 2008; W. C. Hockaday et al. 2009; A. Gaspar et al. 2012; S. Lababidi & W. Schrader 2014; A. K. Huba, K. Huba & P. R. Gardinali 2016; J. Hertzog et al. 2017; W. Kew et al. 2018) and extraterrestrial samples (J. Hertzog et al. 2019; G. Danger et al. 2021, 2022) have demonstrated that a discrimination of different compounds can be observed based on the ionization method used in FT-ICR MS analyses (P. Kebarle & L. Tang 1993; D. B. Robb, T. R. Covey & A. P. Bruins 2000; T. C. Rohner et al. 2004; M. Wilm 2011). During the analysis of a complex matrix, ionization competition can occur between molecules, particularly since ESI favours the detection of highly acidic or basic species, which are not always the most abundant, leading to ion suppression phenomenon. To overcome this limitation, the combination of multiple ionization modes has been proposed as an effective strategy to maximise the characterization of the chemical diversity within complex mixtures (J. Hertzog et al. 2017, 2019).

In this contribution, we pursue on the analysis of SOMA generated from VUV-processed interstellar ice analogues composed of $H_2O$-$CH_3OH$-$NH_3$, using high-resolution FT-ICR mass spectrometry with complementary ionization modes. We use elec-

trospray and atmospheric pressure photoionization (APPI; D. B. Robb et al. 2000) methods in both positive and negative modes. A comparison to Murchison meteorite analyses is also present to determine if this multimodal ionization analysis can give additional similarities between laboratory analogues and extraterrestrial organic matter, potentially providing new information on the origin of the SOM of meteorites.

## 2. MATERIALS AND METHODS

### 2.1. Analogue formation and alteration

In order to form a SOMA (G. Danger et al. 2022), the MICMOC experiment (Matière Interstellaire et Cométaire; Molécules Organiques Complexes) was used at PIIM laboratory (Marseille, France). The interstellar ice analogues were growth using gas mixtures composed of $H_2O$, $CH_3OH$, and $NH_3$ inside of a stainless-steel vacuum line. $H_2O$ was purified using a Millipore Direct Q5 system, $CH_3OH$ was purchased from Sigma–Aldrich (99.96 per cent purity – Hypergrade), and $NH_3$ from Air Liquide (99.96 per cent purity – N36). The gaseous mixture is then deposited onto an inert $MgF_2$ window cooled at 77 K, using liquid nitrogen (Linde Cryovit) in a stainless-steel ultra-high vacuum chamber at a pressure of $10^{-8}$ mbar. Fourier-transform infrared spectroscopy (FT-IR) was used to monitor ice composition and its evolution by following the signals of organics formed through the experiment, using a Bruker Vector 2 infrared spectrometer (4000–400 $cm^{-1}$, 400 scans per spectrum with a 1 $cm^{-1}$ resolution; G. Danger et al. 2022). The spectral absorption bands analysed in this study were extracted from M. Bouilloud et al. (2015, see Fig. S1 and Table S1 in Supporting Information). Ice formation is concomitant to its irradiation with VUV photons (mainly Lyman $\alpha$ – 121.6 nm; H. Cottin, M. H. Moore & Y. Benilan 2003; G. A. Cruz-Diaz et al. 2014) using a microwave-generated $H_2$ plasma lamp. A synchronized deposition and irradiation process allows for an increase in the efficiency of photolysis on the initial compounds, by enabling more material to be processed before being buried by an optical thick layer of ice (J. P. Dworkin et al. 2004). Additionally, the number of photons interacting with the initial matrix can be more precisely controlled (T. Javelle et al. 2024), which is more difficult to achieve with layered ice irradiation. The photon flux was calibrated using replicated actinometry on a methanol ice irradiation, monitoring the CO band of methanol (1047–1006 $cm^{-1}$: $1.8 \times 10^{-17}$ cm molecule$^{-1}$; T. Javelle et al. 2025). A constant photons flux about $3.7 \times 10^{14}$ photons $cm^{-2}$ $s^{-1}$ over 72 h is used, giving a total UV fluence of $9.6 \times 10^{19}$ photons $cm^{-2}$. The flux measured in preliminary experiments is assumed to remain constant across the different experiments. The photo-processed ice is then slowly warmed up to 300 K at a rate of 0.1 K $min^{-1}$, avoiding blasting event inside of the sample (L. L. S. d'Hendecourt et al. 1982), leading to the formation of an organic residue.

In this study, three residues were produced with the following initial compositions in the ice: (1) $H_2O$-$CH_3OH$-$NH_3$ in ratio [3-1-3] (SOMA-1); (2) $H_2O$-$CH_3OH$-$NH_3$ in ratio [3-1-1] (SOMA-2); and $H_2O$-$CH_3OH$-$NH_3$ in ratio [3-1-2] (SOMA-3). This study focuses on the SOMA-1 sample, with SOMA-2 and SOMA-3 serving as control experiments (more information on the three samples is available in Sections S1, S2, and S3 of the Supporting Information). These control experiments were designed to assess the impact of small variations in the initial ice mixture ratios on the chemical composition of the resulting residues.

The infrared windows covered with residues are then removed from the vacuum chamber and stored in a sample holder under a pressure of $10^{-3}$ mbar. To extract the SOMA, the residue is recovered by rinsing the $MgF_2$ window with $3 \times 50$ µL of ultrapure methanol, then 20 µL of this solution are sampled and completed with 200 µL of ultrapure methanol. The extractions were performed immediately prior to analysis to limit as much as possible any chemical reactivity in solution. Methanol is selected here as the solvent, based on previous studies on similar organic residues (G. Danger et al. 2013, 2016, 2021) or extraterrestrial samples (P. Schmitt-Kopplin et al. 2010; N. Hertkorn et al. 2015; A. Ruf et al. 2017; J. Hertzog et al. 2019; D. P. Glavin et al. 2025), which highlights the strength of this solvent in solubilizing a major fraction of their organic matter. For APPI, 20 µL of the stock solution were diluted in 200 µL of a 90:10 (v/v) methanol: acetone mixture. Acetone served as a dopant to assist ionization. The diluted solutions were then used for FT-ICR MS analyses. Residues were analysed across three separate campaigns (SOMA-2 in 06/2024, SOMA-1 in 10/2024, and SOMA-3 in 06/2025), each time in triplicate injections.

### 2.2. FT-ICR MS analysis

#### *2.2.1.* FT-ICR MS

FT-ICR MS analyses of three distinct samples were performed at the LCP-A2MC facility in Metz (France), using a SolariX 2xR (Bruker Daltonics, Bremen, Germany) with a 7-Tesla magnet. Four different ionization modes were employed: ESI (Bruker Daltonics) and APPI (Bruker Daltonics), each operated in both negative- and positive-detection modes. Optimization of the ion source and instrumental parameters was performed using the FTMS-Control v2.3.0 software (Bruker Daltonics). Prior the analyses, an external calibration was performed on the mass spectrometer, and the ICR detection cell is shimmed and gated using a 0.1 mg $mL^{-1}$ sodium trifluoroacetate solution.

Mass spectra were recorded within a mass range from *m/z* 107.5 to 1500, with an 8 megaword time-domain, and resulted from the accumulation of several scans, depending on the ionization mode, and detailed in the next sections. Mass resolutions of 1 000 000, 600 000, and 400 000 were achieved at *m/z* 200, 400, and 600, respectively.

#### *2.2.2.* ESI (+)/(−) analyses

In this work, the ESI was employed in both negative- and positive-ion modes. The solution was infused at a flow rate of 3 $\mu$L $min^{-1}$ for both modes. The drying gas temperature was maintained at 200 °C with a flow rate of 4 L $min^{-1}$, and the nebulizer gas pressure was set to 0.5 bar. For positive-ion mode, a capillary voltage of 3.9 kV was applied, whereas for negative-ion mode, a voltage of 3.7 kV was used. For ESI (+), 200 scans were acquired for the SOMA-1 sample and 250 scans for SOMA-2 and SOMA-3. For ESI (−), 400 scans were accumulated for the three samples. An ion accumulation time of 0.020 s was applied in both ionization modes.

#### *2.2.3.* APPI (+)/(−) analyses

APPI source, equipped with a krypton lamp that emits 10.6 eV photons, was employed in this experiment with both negative-

and positive-ion modes. APPI (−) was only used for the SOMA-1 sample. The samples were infused at a flow rate of 5 $\mu$L min$^{-1}$. The drying gas temperature was maintained at 220 °C with a flow rate of 4 L min$^{-1}$, and the nebulizer gas pressure was set to 2.5 bar in positive mode and 4 bar in negative mode. A capillary voltage of 0.8 kV was applied for both modes. The source temperature was set at 400 °C. For APPI (+), 250 scans were acquired for the three samples, with an ion accumulation time of 0.1 s for SOMA-1 and SOMA-3 and 0.020 s for SOMA-2. For APPI (−), 250 scans were accumulated, with an ion accumulation time of 0.1 s.

### 2.3. MS data analysis

#### *2.3.1.* Molecular assignment

Internal calibration of the FT-ICR mass spectra was performed using DataAnalysis 5.0 software (Bruker, Daltonics), using a mass list of compounds known to be present in interstellar ice analogues with unambiguously assigned molecular formulas, and a standard deviation of mass error ≤ 100 ppb. The list of lock masses used for each analysis can be found in the Table S2 in Supporting Information. For each mass spectrum, a mass list of ions with signal-to-noise ratio ≥ 6 were extracted and aligned with a 0.5 ppm tolerance window. Molecular assignment of the resulting peak lists was then performed with COMPOSER software (Sierra Analytics, Modesto, USA), with a ± 0.2 ppm tolerance for ESI (+), APPI (+), and APPI (−) and with a ± 0.3 ppm tolerance for ESI (−). For each ionization mode, molecular formulas were assigned with the C (≥5), H, N (≤20), and O (≤20) elements. Soft ionization mode, such as electrospray, can lead to the formation of adducts ions by the interaction of a precursor ion with one or more atoms or molecules, present intentionally or unintentionally in the sample solution. Different ion types were considered here with $[M + H]^+$, $[M + Na]^+$, and $[M + K]^+$ ions for ESI (+); $[M\text{-}H]^-$ and $[M + Cl]^-$ for ESI (−); $[M + H]^+$, $[M]^{\bullet+}$ and $[M\text{-}H]^-$, $[M]^{\bullet-}$ for APPI (+) and APPI (−), respectively. In the case of ESI (+), the distribution of ion types was as follows: $[M + H]^+$ accounted for 66 per cent of the assignments, $[M + Na]^+$ for 26 per cent, and $[M + K]^+$ for 8 per cent. For ESI (−), $[M\text{-}H]^-$ was the predominant ion type, representing 97 per cent of the assignments, while $[M + Cl]^-$ contributing 3 per cent. In APPI (+), no radical cations $[M]^{\bullet+}$ were detected, while in APPI (−), radical anions $[M]^{\bullet-}$ accounted for 1 per cent of observed species. $Na^+$, $K^+$, and $Cl^-$ ions originate from the solvents, bottles, and glassware used as part of the sample preparation, and cannot be fully avoided.

For each analytical condition, an instrument blank, corresponding to the analysis of the dilution solvents (methanol and acetone) alone, was acquired with the same acquisition parameters, in order to observe potential contaminants that can be further found in the sample mass spectra. When observed, the corresponding peaks/signals were retrieved to keep signals relating to samples. Furthermore, features present in the mass spectra of blanks, with a sample-to-blank intensity ratio lower than 3, were excluded from the mass list.

Analytical repeatability was evaluated using coefficients of variation (CV) calculated for the intensity of each detected mass across the three replicate injections of a same sample. Table S3 in Supporting Information provides detailed percentages of assignments with CVs below 10 per cent, 20 per cent, and 30 per cent. Overall, triplicate injections resulted in an average analytical variability of 8 per cent, 7 per cent, 7 per cent, and 9 per cent for ESI (+), ESI (−), APPI (+), and APPI (−), respectively. Furthermore, approximately 70 per cent of the mass detected exhibited CVs below 10 per cent, 95 per cent below 20 per cent, and 99 per cent below 30 per cent, demonstrating an outstanding stability of the FT-ICR MS measurements. The variability in the total number of molecular formulas between triplicates was less than 1 per cent, indicating that instrumental variability is minimal and cannot account for the molecular diversity differences observed between samples. Therefore, the slight variations observed between the three samples are attributed to the minor compositional differences in the initial ice mixtures, as discussed in Section 4.2.

#### *2.3.2.* Data treatment

Compounds were categorized into CH, CHO, CHN, and CHNO groups, based on their elemental composition. Fig. 1(a) gathers van Krevelen diagrams representing the H/C and O/C or H/C and N/C ratios of the different compound classes identified in the SOMA-1 [3-1-3] obtained with the four ionization modes. To facilitate interpretation, a van Krevelen diagram can be expressed in terms of discrete biochemical structural classes, originally defined from natural organic matter analyses (R. L. Sleighter & P. G. Hatcher 2007; N. Hertkorn et al. 2008; W. C. Hockaday et al. 2009; T. Ohno et al. 2010; E. Wollrab et al. 2016). These classes were then adapted to an astrophysical context, reflecting the biochemical families commonly identified in icy analogues (M. P. Bernstein et al. 1995; G. M. Muñoz Caro et al. 2002; G. M. Muñoz Caro & W. A Schutte 2003; G. Danger et al. 2013, 2016; P. De Marcellus et al. 2015; C. Meinert et al. 2016; M. Nuevo et al. 2018) and in extraterrestrial samples (P. Schmitt-Kopplin et al. 2010; N. Hertkorn et al. 2015; Y. Furukawa et al. 2025; A. Mojarro et al. 2025). This mapping approach does not aim to identify specific molecules but rather provides an overview of the sample diversity. Eight categories (see Fig. S2 in Supporting Information) are defined as follows: (i) category 1 includes fully saturated species (H/C ≥ 2.0 and 0 ≤ O/C < 2), ranging from hydrocarbons to alcohols, not included in categories 2a, 2b, and 2c; (ii) category 2a encompasses long alkyl chains with aldehyde or carboxylic acid functions, such as lipid-like structures (1.5 ≤ H/C < 2.5 and 0 ≤ O/C < 0.3); (iii) category 2b contains long alkyl chains with moderate oxygen and nitrogen content, such as amino acids (1.5 ≤ H/C < 2.8 and 0.3 ≤ O/C < 0.65); (iv) category 2c comprises oxygen-enriched molecules, such as carbohydrate-like compounds, with low nitrogen content (1.5 ≤ H/C < 2.4 and 0.65 ≤ O/C < 2); (v) category 3a represents unsaturated hydrocarbons, possibly containing phenyl groups, with lower oxygen content and enriched in nitrogen (0.75 ≤ H/C < 1.5 and 0 ≤ O/C < 0.1); (vi) category 3b corresponds to lignin-like structures, with unsaturated structures link with ether bonds (0.75 ≤ H/C < 1.5 and 0.1 ≤ O/C < 0.65); (vii) category 3c includes weakly aromatized structures that are oxygen-enriched and nitrogen-depleted (0.75 ≤ H/C < 1.5 and 0.65 ≤ O/C < 2); and (viii) category 4 consists of condensed aromatic structures containing both oxygen and nitrogen functions (0.2 ≤ H/C < 0.65 and 0 ≤ O/C < 0.65).

The bubble size refers to the signal intensity and the colour to the double bond equivalent (DBE) value from 0 to 20. The DBE was calculated for each molecular assignment $C_wH_wN_yO_z$, using the following formula: $\mathrm{DBE} = n(\mathrm{C}) - \frac{n(\mathrm{H})+n(\mathrm{N})}{2} + 1$, where $n$(X) is number of specific atoms present in the molecule.

The DBE offers insights into the number of rings and unsaturations in a molecule. In addition, the aromaticity equivalent

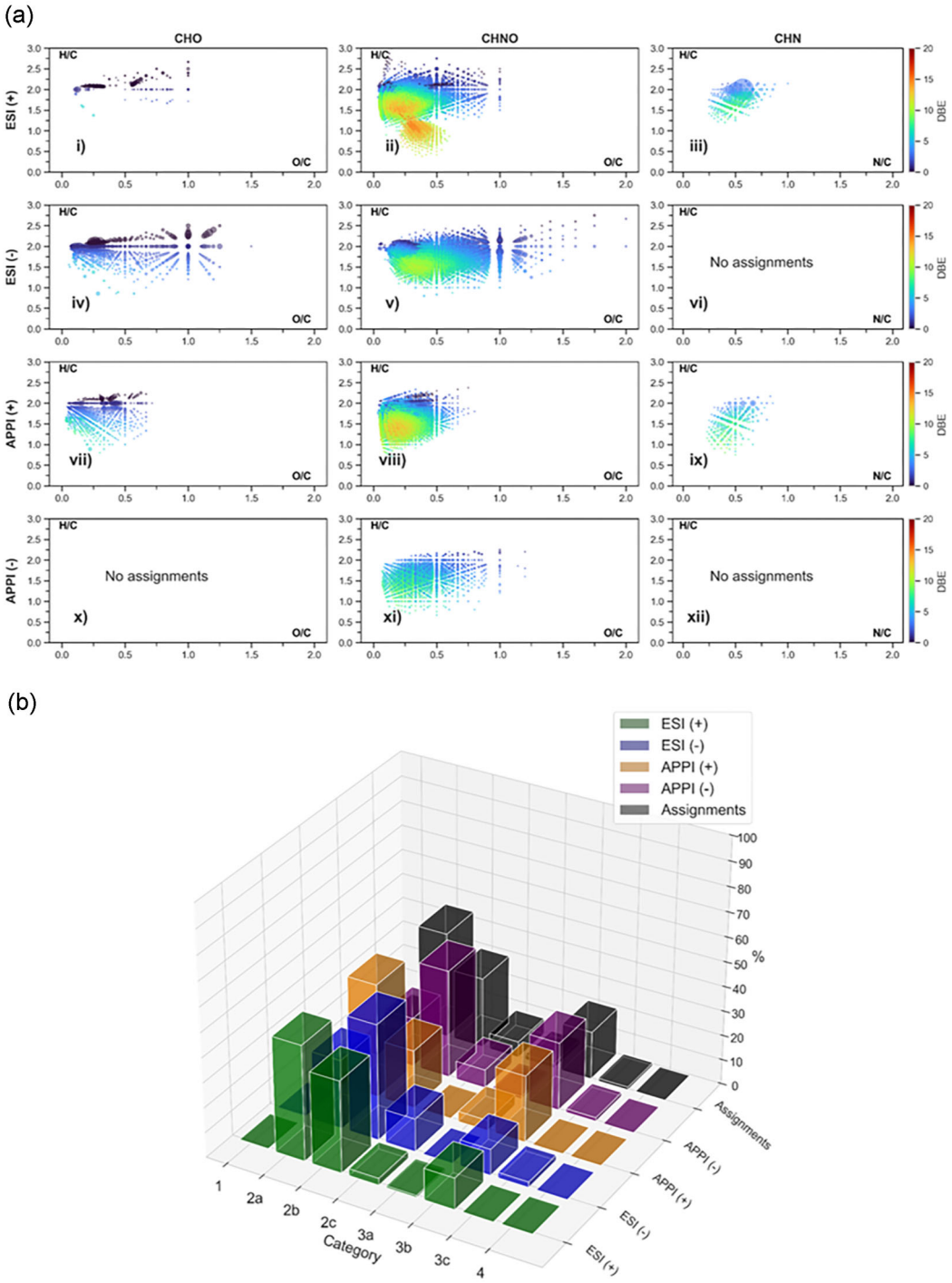


**Figure 1.** (a) van Krevelen diagrams of the different heteroatom classes identified in the SOMA-1, with multiple ionization modes ESI (+), ESI (−), APPI (+), and APPI (−). The bubble size refers to the signal intensity. (b) Distribution of the van Krevelen categories for each ionization mode used, as well as the total number of molecular formulas detected, referred as 'Assignments', based on G. Danger et al. (2016) partitions. Category 1: fully saturated structures -OR/-$NR_1R_2$. Category 2a: alkyl chains with $CO_2H$/$CONH_2$. Category 2b: alkyl chains (-$CO_2R$)n/(-$CONR_1R_2$)n/-$NR_1R_2$. Category 2c: alkyl chains enriched in O (-$CO_2R$)n/-OR with low amount of N. Category 3a: conjugated structures with possible phenyl groups enriched in N with few O functions. Category 3b: conjugated structures with possible phenyl groups (-$CO_2R$)n/(-$CONR_1R_2$)n/-$NR_1R_2$. Category 3c: conjugated structures with possible phenyl groups, enriched in O with few N functions. Category 4: highly aromatic structures with O and N functions.

parameter $X_c$, based on M. M. Yassine et al. (2014), was also calculated as follows: $X_c = \frac{2n(\mathrm{C})+n(\mathrm{N})-n(\mathrm{H})-2m\times n(\mathrm{O})}{\mathrm{DBE}-m\times n(\mathrm{O})} + 1$. If DBE $\leq m \times n(O)$, then $X_c = 0$.

Here, $m$ represents the fraction of oxygen atoms involved in the $\pi$-bond structure of the compound. This fraction was assumed to be equal to 0.5, based on molecular composition observed in prior studies employing infrared spectroscopy and FT-ICR MS analysis of similar residues (G. M. Muñoz Caro & W. A Schutte 2003; G. Danger et al. 2013, 2022). Using the calculated $X_c$ parameter, three chemical classes can be defined: assignments with

**Table 1** Description of the SOMA-1 extracted from $H_2O$-$CH_3OH$-$NH_3$ [3-1-3] analogue sample, analysed by ESI-FT-ICR MS in positive and negative modes, and APPI in positive and negative modes. Number of assignments for each class of molecules (CH, CHO, CHN, and CHNO), percentages of atomic ratios, as well as the average DBE, $X_c$, mass, and formula for each analytical condition are also displayed.

| Heteroatom class | ESI (−) | ESI (+) | APPI (+) | APPI (−) |
|---|---|---|---|---|
| CH | – | – | 4 (0.1 per cent) | – |
| CHO | 692 (9.4 per cent) | 199 (1.5 per cent) | 713 (10.5 per cent) | – |
| CHN | – | 243 (1.8 per cent) | 233 (3.4 per cent) | – |
| CHNO | 6697 (90.6 per cent) | 12 932 (96.7 per cent) | 5827 (86.0 per cent) | 2165 (100.00 per cent) |
| Total assigned features | 7389 | 13 374 | 6777 | 2165 |
| Average O/C | 0.44 | 0.30 | 0.24 | 0.39 |
| Average H/C | 1.76 | 1.72 | 1.61 | 1.60 |
| Average N/C | 0.28 | 0.39 | 0.28 | 0.39 |
| Average DBE | 5 | 7 | 7 | 6 |
| Average $X_c$ | 1.38 | 2.18 | 2.16 | 2.09 |
| Average mass | 389.15 172 | 427.23 508 | 358.79 860 | 318.26 309 |
| Average formula | $C_{16}H_{29}N_4O_6$ | $C_{18}H_{30}N_7O_5$ | $C_{17}H_{27}N_5O_4$ | $C_{13}H_{21}N_5O_5$ |

$0 \leq X_c < 2.5$ are categorized as aliphatic; compounds with $2.5 \leq X_c < 2.7$ are considered as aromatics, with a benzene-like structure ($C_6H_6$–$X_c = 2.50$); and compounds with an $X_c$ index higher or equal to 2.7 are classified as condensed aromatics, characterized by multiple rings and unsaturated features (naphthalene $C_{10}H_6$–$X_c = 2.71$; M. M. Yassine et al. 2014).

## 3. EXPERIMENTAL RESULTS

### 3.1. ESI (−) FT-ICR MS analysis

The ESI (−) analyses of SOMA-1 enabled the assignment of over 7000 molecular formulas (Table 1), including approximately 91 per cent CHNO and 9 per cent CHO compounds. No CHN compounds were identified using ESI (−) ionization source.

On average, this ionization mode exhibits the highest O/C ratio (0.44). As observed from the van Krevelen H/C versus O/C diagram (Fig. 1a) van Krevelen diagrams of the different heteroatom classes identified in the SOMA-1, with multiple ionization modes ESI (+), ESI (−), APPI (+), and APPI (−). The bubble size refers to the signal intensity and the colours to the DBE value from 0 to 20, and (b) distribution of the van Krevelen categories for each ionization mode used, as well as the total number of molecular formulas detected, referred as 'Assignments', based on G. Danger et al. (2016) partitions. Category 1: fully saturated structures -OR/-NR1R2. Category 2a: alkyl chains with CO2H/CONH2. Category 2b: alkyl chains (-CO2R)n/(-CONR1R2)n/-NR1R2. Category 2c: alkyl chains enriched in O (-CO2R)n/-OR with low amount of N. Category 3a: conjugated structures with possible phenyl groups enriched in N with few O functions. Category 3b: conjugated structures with possible phenyl groups (-CO2R)n/(-CONR1R2)n/-NR1R2. Category 3c: conjugated structures with possible phenyl groups, enriched in O with few N functions. Category 4: highly aromatic structures with O and N functions. (a) – (iv) and (v), ESI (−) indeed gives the largest chemical space, with O/C values ranging from 0.05 to 2.0, and a significant number of assignments in the fatty acid region (H/C > 1.50 and O/C < 0.25; category 2a). Most of the features shows H/C ratio higher than 1.5, with an average of 1.76, emphasizing the aliphatic nature of these species.

In addition, more than 35 per cent of the molecular formulas present an O/C greater than 0.5 and almost 4 per cent higher than 1.0. This underlines the efficiency of the chosen ionization mode in detecting acidic, highly oxidized compounds with a low degree of unsaturation (average DBE = 5 and average $X_c = 1.38$). In these ice analogues, a part of the organic diversity detected by the ESI (−) analyses might range from aliphatic structure, such as carbohydrates and polyols, to molecules presenting some unsaturated features such as fatty acids or amino acids, in agreement with previous studies (G. Danger et al. 2013, 2016, 2021, 2022; C. Meinert et al. 2016; M. Nuevo et al. 2018). Aromatic compounds, possibly corresponding to phenols or polyphenols, were also detected (22 per cent of the molecular assignments with $X_c \geq 2.5$).

The CHNO chemical class dominates the ESI (−) distribution with 6697 features (91 per cent). Approximately 76 per cent of these CHNO assignments (5085 formulas) exhibit an aromaticity degree ($X_c$) value below 2.5 and are classified as aliphatics. Among them, two categories can be distinguished: (a) 2975 assignments exhibiting few unsaturations ($1 \leq X_c < 2.5$), with similar characteristics than the overall distribution and thus a high incorporation of heteroatoms; (b) 2110 saturated compounds ($X_c < 1$), highly oxygenated (O/C = 0.57) characterized by slightly lower ion masses (average of $m/z$ 371.68793) and a slight decrease of the N/C ratio (0.23). These results suggest the presence of species likely composed of alkyl chains with few unsaturation and saturated oxygen- and nitrogen-bearing functional groups, such as alcohols, carboxylic acids, amides, amines, amino acids or aldehydes (categories 2a, 2b, 2c – Fig. 1b). High degrees of oxygenation are achieved with O/C ratio reaching up to 2.0. Assignments with O/C above 1.0 are primarily classified within the $N_2O_z$, $N_3O_z$, and $N_4O_z$ classes, containing between 4 and 11 oxygen atoms. All of these compounds belong to the aliphatic class (DBE = 2; $X_c = 0.02$) and were consistently detected as deprotonated ions $[M\text{-}H]^-$, indicating the presence of labile acidic functional groups. From an acidity viewpoint, imides (R-CO-NH-CO-R'; DBE = 2), hydrazides (R-CO-NH-NH-R'; DBE = 1), and semicarbazides (R-CO-NH-NH-CO-$NH_2$; DBE = 2), among others, are significantly more acidic, with typical pKa values ranging from 6 to 11. Such functionalities, characterized by high heteroatom content, therefore represent plausible candidate structures and are readily detectable in ESI (−). Combined with their high oxidation state, these observations suggest the potential presence of nitrogen-containing functionalities, such as alkyl nitrites or nitro groups,

alongside secondary and tertiary amines, together with labile groups.

Approximately 24 per cent of CHNO assignments (1612) can be regarded as aromatics and condensed aromatics ($X_c \geq 2.5$). Within this group two distinct distributions can be distinguished. The first comprises 514 formulas with H/C ratios below 1.5, characterized by a lower nitrogen content (average N/C ratio = 0.31), and an average ion mass of *m/z* 370.53747. The second distribution includes compounds with an H/C ratio greater than 1.5, exhibiting extended carbon chains (*m/z* 454.99989), and higher nitrogen incorporation (N/C = 0.41). For this latter category, structures involving long alkyl chains bearing acidic N-heterocycles, such as aromatic imides, imidazoles, pyrazoles, triazoles, or tetrazoles, may explain the observed molecular formulas.

The aliphatic or aromatic nature of CHNO structures appears to be influenced by their nitrogen content. Higher nitrogen content often correlates with an increase of the $X_c$ parameter and thus an increased aromaticity, suggesting substantial nitrogen incorporation into unsaturated or aromatics moieties, while aliphatic structures tend to have a greater oxygen content. This trend also seems to be related to molecular size, with lower mass molecules being more aliphatic and oxidized, while higher mass CHNO species exhibit greater aromaticity and a nitrogen enrichment.

Regarding the CHO compounds, 692 formulas (9 per cent) were attributed. These molecules are mostly aliphatic structures (97 per cent of formulas with $X_c < 2.5$), with a moderate oxygen content (O/C = 0.44) and a low degree of unsaturation (H/C = 1.84; DBE = 2; and $X_c = 0.36$; Fig. 2). The oxygen distribution spans from one to twelve oxygen atoms per formula (see Fig. S3 in Supporting Information), with an average ion mass of *m/z* 310.77878. Based on previous studies of such residues, these compounds are likely composed of multiple saturated oxygenated functions such as hydroxyl group, and might be related to carbohydrates, fatty acids, polyols, or carboxylic acids (C. Meinert et al. 2016; M. Nuevo et al. 2018).

### 3.2. ESI (+) FT-ICR MS analysis

The ESI (+) analyses of the SOMA-1 were able to assign 13 374 formulas. The positive mode is well-adapted to basic nitrogen-containing species (A. Gaspar et al. 2012; S. Lababidi & W. Schrader 2014; W. Kew et al. 2018; G. Danger et al. 2021), exhibiting the highest N/C ratio (0.39) among the four analytical conditions. It also detects heavier species, with the highest average *m/z* of 427.23508 and the greatest average unsaturation degree, as indicated by the average aromaticity index of 2.18 and DBE of 7.

ESI (+) analyses provide the detection of CHNO molecules including nitrogen- and oxygen-containing classes, spanning from $N_1O_z$ to $N_{15}O_z$ and from $N_yO_1$ to $N_yO_{11}$ (see Fig. S3 in Supporting Information). The van Krevelen diagram (Fig. 1a-ii) shows that features are mainly concentrated in regions characterized by medium to low H/C ratios. This mode detects alkyl chains with moderate oxygen content, with an average O/C around 0.30 (Fig. 1b; category 2a and 2b), along with unsaturated compounds from the 3b category, which likely possess conjugated structures with oxygen-containing basic functional groups.

Similar to ESI (−) results, ESI (+) data are dominated by the CHNO chemical class with 97 per cent of the formulas assigned. In the present case, the $X_c$ profile of CHNO compounds differs from ESI (−) (Fig. 2): (i) aromatics or condensed aromatics compounds ($X_c \geq 2.5$) dominate with 7661 (59 per cent of CHNO species) molecular formulas; and (ii) aliphatic group ($X_c < 2.5$) comprises 5271 (41 per cent) formulas, including 3981 (31 per cent) assignments with $1 \leq X_c < 2.5$ and 1290 (10 per cent) features with $X_c < 1$.

The most aromatic assignments ($X_c \geq 2.5$) are 'high-mass' species (*m/z* 485.03762), highly polar with a significant number of heteroatoms (H/C = 1.60; O/C = 0.25; and N/C = 0.40), containing an average of five oxygen and eight nitrogen atoms per formula. In this group, assignments with H/C ratios below 1.5 are characterized by lower average mass (*m/z* 389.31934), with an important unsaturation degree (H/C = 1.21; DBE = 8; and $X_c = 2.62$), a slightly higher oxygen content (O/C = 0.30) and a reduced nitrogen content (N/C = 0.26). This subset likely consists of highly condensed aromatic molecules, potentially with multiple phenyl groups and a lower number of heteroatoms. In contrast, the second distribution with an H/C ≥ 1.5 presents an average mass of *m/z* 512.19095, a lower oxidation degree (O/C = 0.23) and a pronounced nitrogen incorporation (N/C = 0.44), similar to what was observed in ESI (−). Compounds with an $X_c$ value greater than 2.5 and higher value of H/C reflect the presence of extended carbon chains bearing multiple basic and unsaturated functionalities, specifically nitrogen-containing groups, such as amines, amides, lactams, hydrazines, nitriles, imines, oximes, pyridine, or aniline. Unsaturation is thus mainly associated with nitrogen-rich structures and higher ion masses. Moderate unsaturated molecules ($1 \leq X_c < 2.5$) and aliphatic compounds ($X_c < 1$) tend to incorporate a higher number of oxygenated groups with O/C ratios of 0.35 and 0.51, respectively, such as ester and ether. Meanwhile, the N/C ratios decrease (0.40 and 0.27, respectively) with declining aromaticity and average ion mass (*m/z* 367.55065 and 312.57179, respectively).

A distinct family of highly unsaturated compounds is observed in the van Krevelen diagram (Fig. 1a-ii) for CHNO species detected in ESI (+), characterized by DBE values greater than 10 and H/C ratios below 1.25. This group accounts for 713 CHNO features (6 per cent) and seems to be condensed aromatic structures (H/C = 0.99; DBE = 12; and $X_c = 2.76$), depleted in nitrogen (N/C = 0.17). Notably, this family is absent in SOMA-2 and SOMA-3, likely due to the lower ammonia content in the initial ice mixture of the SOMA-1.

Regarding CHO class, 199 assignments were obtained. All the CHO formulas were detected through adduct addition, with 106 formulas (53 per cent) exhibiting a sodium adduct $[M + Na]^+$ and the remaining formulas as potassium adduct $[M + K]^+$, with average masses of *m/z* 338.10569 and 367.22039, respectively. Such adducts are likely formed through interactions involving functional groups bearing heteroatoms with lone pairs (Lewis-acid-base reaction; A. Kruve et al. 2013). The vast majority (99 per cent) are classified as aliphatic (DBE = 0.5 and $X_c = 0.05$; Fig. 2), with high hydrogen content (H/C = 2.08) and significant amount of oxygen (O/C = 0.48; an average of 6 oxygen atoms per formula). CHO species are detected among a wide range of chemical classes, containing oxygen atoms from 2 to 10 (see Fig. S3 in Supporting Information). The van Krevelen diagram (Fig. 1a-i) places most of CHO features within categories of low- to moderately oxygenated alkyl chains (2a and 2b), with O/C values up to 1.0. Their low DBE and high H/C values support a predominance of saturated oxygenated functionalities, likely consisting of long alkyl chains, with abundant hydroxyl and ether groups, alongside smaller amounts of unsaturated groups such as esters.

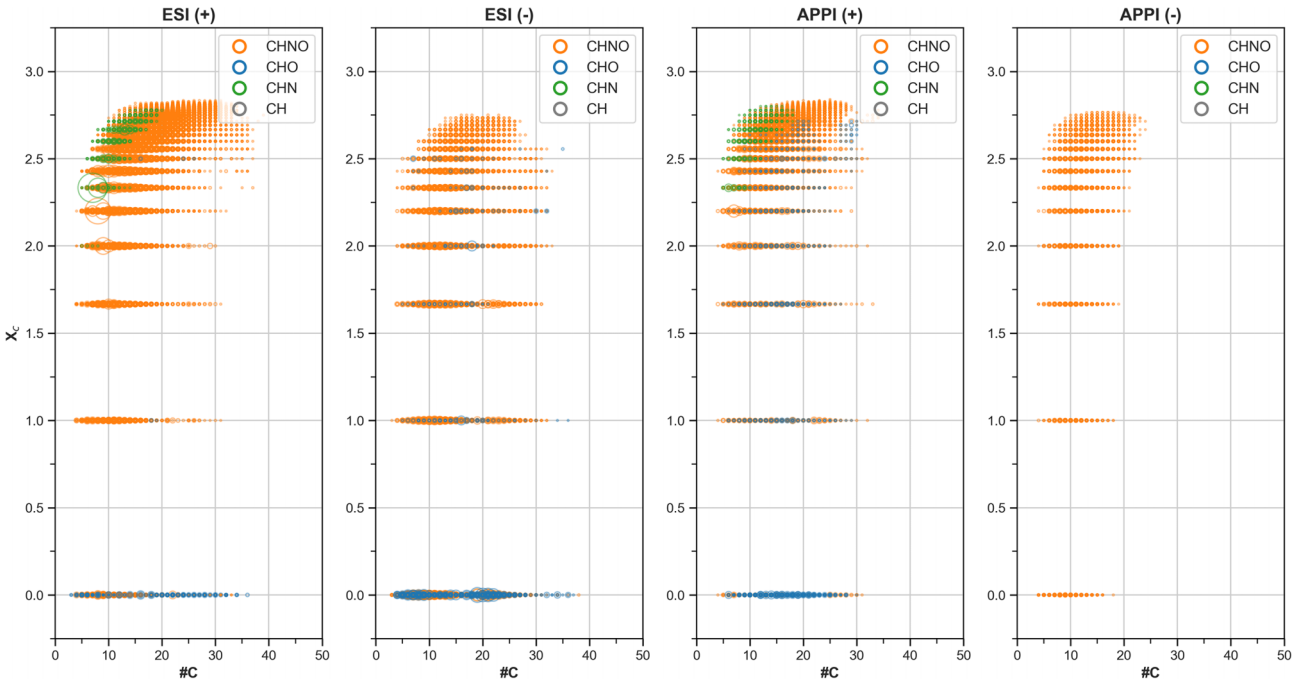


**Figure 2.** Aromaticity equivalent distributions of molecular formulas in the SOMA-1 sample, achieved by ESI (+), ESI (−), APPI (+), and APPI (−). The bubble size refers to the signal intensity. An $X_c$ value of 2.5 would be analogue to a benzene-like structure.

The CHO formulas exhibiting a high hydrogen and oxygen content with a single degree of unsaturation (DBE = 1) may correspond to monosaccharide, including aldoses, ketoses or sugar acids (C. Meinert et al. 2016). On the van Kreleven diagram (Fig. 1a-i), a denser cluster of assignments is observed in the region of low oxygen content (2a), which could represent fatty acids, as supported by the presence of long carbon chains ($C_8$ to $C_{20}$) bearing 2 oxygen atoms, such as: $C_8H_{16}O_2Na^+$ (*m/z* 167.10423) or $C_{20}H_{40}O_2Na^+$ (*m/z* 335.29204). Compounds with a DBE of 2 were also detected (15 formulas), which may correspond to the signature of dicarboxylic acids. As carbohydrates were detected by GC-MS analysis of similar residue, the presence of glycolipids is also likely. Finally, ESI (+) provides the detection of saturated and aliphatic CHO with DBE equal to 0 and several oxygen atoms (categories 2b and 2c), such as dipropylene glycol, which might be detected here as $C_6H_{14}O_3K^+$ at *m/z* 173.05745 (0.0152 ppm error).

In the CHN class, 243 formulas (2 per cent) were assigned. The detected nitrogen-bearing compounds may predominantly be low-mass aromatics (*m/z* 253.26546; $X_c = 2.61$), exhibiting great H/C ratio (1.72), with high amount of nitrogen (N/C = 0.49). Their N/C ratios range from 0.25 to 1, and the $X_c$ values between 2 and 2.78, suggesting unsaturated/aromatic structures (Fig. 2) with extensive nitrogen incorporation, via functional groups including nitriles, imines, anilines, or N-heterocycles such as pyridine. These observations are consistent with previous studies reporting the presence of hexamethylenetetramine (HMT – $C_6H_{12}N_4$; H/C = 2; N/C = 0.67; $X_c$ = 2.33; and DBE = 3) in similar organic residues (G. M. Muñoz Caro et al. 2004; G. Danger et al. 2013; A. Garcia 2023), which is detected here at the *m/z* 141.11343, as one of the most intense peaks in the mass spectrum. Regarding the HMT-derivatives, $C_8H_{16}N_4O$, previously reported by G. Danger et al. (2013), was detected in our experiment at *m/z* 185.13968. Twelve additional HMT-related compounds ($[M + H]^+$) can be proposed, consistent with previous chromatographic studies by G. M. Muñoz Caro *et al.* (2004), A. Garcia (2023), and C. del Burgo Olivares *et al.* (2025): HMT-$CH_3$ ($C_7H_{14}N_4$) at *m/z* 155.12912; HMT-OH ($C_6H_{12}N_4O$) at *m/z* 157.10838; HMT-$CH_2CH_3$ ($C_8H_{16}N_4$) at *m/z* 169.14477; HMT-$CH_2NH_2$ ($C_7H_{15}N_5$) at *m/z* 170.14002; HMT-$CH_2OH$ ($C_7H_{14}N_4O$) at *m/z* 171.12403; HMT-CO-$CH_3$ and HMT-$CH_2$-CHO ($C_8H_{14}N_4O$) at *m/z* 183.12403; HMT-NH-CHO ($C_7H_{13}N_5O$) at *m/z* 184.11928; HMT-O-CHO ($C_7H_{12}N_4O_2$) at *m/z* 185.1033; HMT-$CH_2$-CO-$CH_3$ and HMT-$C_2H_4$-CHO ($C_9H_{16}N_4O$) at *m/z* 197.13969; HMT-NCO ($C_7H_{11}N_5O$) at *m/z* 198.09855; HMT-CHOH-CHO ($C_8H_{14}N_4O_2$) at *m/z* 199.11895; and HMT-$CH(CH_3)$-$CH_2NH_2$ ($C_9H_{19}N_5$) at *m/z* 214.16623. Further MS/MS analyses are required to confirm the identity of these ions by searching fragment consistent with HMT structure.

ESI enables the detection of a wide range of organic compounds from the SOMA. Nevertheless, it introduces several biases affecting signal intensity (I. Omari et al. 2019). While it provides high sensitivity due to acid-base chemistry and analyte proton affinities, the most readily ionized are not necessarily the most abundant. First, low-mass compounds are often over-represented in contrast with higher mass species. The nature and pH of the solvent significantly influence ionization efficiency. Depending on their properties, solvents may facilitate ionization or, conversely, form strong intermolecular interactions with analytes, reducing their ionization efficiency and leading to their under-representation (J. Liigand, A. Laaniste & A. Kruve 2017; I. Omari et al. 2019). ESI also involves competition among analytes: highly basic molecules preferentially capture available protons, thereby reducing the ionization efficiency of less basic species. Conversely, in negative mode, the most acidic compounds are favoured. As a result, ESI is particularly sensitive to polar molecules and may therefore limit the detection of the full extent of the organic molecular diversity present in the samples. For these reasons, an additional ioniza-

tion method, APPI, was employed in the following section to determine whether complementary information on SOMA could be obtained.

### 3.3. APPI (+) FT-ICR MS analysis

APPI relies primarily on the absorption of UV light by the solvent (methanol), or a dopant commonly introduced (acetone), as the direct photoionization process of the molecule is generally inefficient. Protonation then often occurs in gas phase via proton transfer involving the solvent, the dopant, or even solvent clusters. As a result, APPI generally reduces the compound-specific biases observed with ESI, providing a complementary overview of the sample molecular composition.

A total of 6777 molecular formulas were assigned by using APPI (+) ionization mode (Table 1). CHNO class represents the dominant group, accounting for about 86 per cent of the distribution. This consistency among the four ionization modes suggests that the prevalence of CHNO compounds reflects the overall diversity of the sample. Additionally, CHO and CHN compounds account for approximately 11 per cent and 3 per cent of assigned formulas, respectively, comparable with CHO distribution identified using ESI (−) and CHN compounds detected in ESI (+) analyses.

As expected, APPI (+) demonstrates particular sensitivity toward aromatic and unsaturated species, as evidenced by the significant representation of categories 3a and 3b, accounting for 4 per cent and 27 per cent of the assignments, respectively. These values exceed those observed in ESI (+) (1 per cent and 13 per cent) and ESI (−) (0 per cent and 10 per cent) (Fig. 1b). Conversely, category 2b, among the most intense in ESI, appears less abundant in APPI (+), whereas category 2a remains consistently represented. The ion population remains largely dominated by alkyl chains with relatively low heteroatom content. Notably, the $N_1O_z$ chemical class dominates the CHNO distribution (see Fig. S3 in Supporting Information), representing the most abundant class (19 per cent) in APPI (+).

Among the CHNO group, 2095 molecular formulas (36 per cent) are classified as aliphatic, while the remaining 3732 assignments (64 per cent) are identified as aromatics or condensed aromatic compounds. Aromatic species with H/C ratio lower than 1.5 (1702 formulas; 29 per cent) present characteristics of slightly smaller molecules (average mass of $m/z$ 358.89696) with reduced nitrogen content (N/C = 0.28). In contrast, aromatic compounds with H/C > 1.5 may correspond to higher mass species ($m/z$ 430.19816), with increased polarity through a greater nitrogen incorporation (N/C = 0.41) into extended carbon chains possibly through saturated functional group such as amine or lactame. It is noteworthy that the oxygen content remains relatively low (O/C ≈ 0.20).

Aliphatic CHNO compounds show distinct trends depending on their degree of unsaturation. Assignments with moderate unsaturation ($1 \leq X_c < 2.5$; 1591 formulas – 12 per cent) are characterized by moderate heteroatom content (H/C = 1.75; O/C = 0.31; and N/C = 0.27), while more saturated species ($X_c <$ 1; 504 attributions) display higher oxygen and hydrogen incorporation (H/C = 1.95 and O/C = 0.38) and contain less nitrogen (N/C = 0.13), for a slightly higher average ion mass ($m/z$ 320.93020 and 339.78140, respectively). As in ESI analyses, unsaturation correlates with nitrogen-rich structures and higher ion masses.

Across all categories, CHNO compounds detected in APPI (+) exhibit reduced heteroatom content and reduced average mass compared to those observed in ESI (+) and ESI (−). This highlights APPI (+) sensitivity toward low-molecular-weight, low-polarity molecules.

The CHO group comprises 713 assigned molecular formulas. In contrast to CHO attributions detected using electrospray in positive mode, these molecules present characteristics of shorter alkyl chain (average ion mass of $m/z$ 296.80158) with higher unsaturation degree (H/C = 1.72 and DBE = 3) and few oxygen atoms per formulas (O/C = 0.27), such as ester or ether. Additionally, APPI (+) analyses led to 125 CHO-assignments (18 per cent) classified as aromatics ($X_c \geq 2.5$) (Fig. 2). Among these, two distinct distributions can be observed: (1) molecules with an H/C below 1.5, consisting of lower mass compounds ($m/z$ 257.26401), highly unsaturated (DBE = 6 and $X_c$ = 2.60), likely bearing phenyl groups, with a decrease of the oxygen amount (O/C = 0.19) with aromaticity. The second family is related to molecules with an H/C value higher than 1.5, with longer unsaturated carbon chains ($m/z$ 364.02774), which are oxygen-depleted (O/C = 0.09). This group predominantly contains molecules bearing two oxygen atoms, likely incorporated into the aromatic ring, such as furan-like compounds, or introduced through carbonyl groups, phenol groups, quinones, or cyclohexadienone-like structures.

For the CHN class, in contrast with ions detected using ESI (+), 233 formulas were assigned, with lower H/C ratio (1.53) and similar N/C ratio (0.47). A population of low-mass (average of $m/z$ 229.02727) molecules with higher aromaticity ($X_c$ = 2.65) is then emphasized. A total of 216 assignments (93 per cent of the CHN class) belongs to the aromatic and condensed aromatic categories (Fig. 2), highlighting again the high degree of unsaturation characteristic of CHN compounds present in residues, and suggesting the presence of aromatic N-heterocycles such as pyridine derivatives. These raw formulas present an average of 5 nitrogen atoms per formula, with a distribution of nitrogen concentrated between 3 and 8 nitrogen atoms per compound (see Fig. S3 in Supporting Information). Concerning HMT-derivatives, APPI (+) allowed the detection of all the derivatives previously observed with ESI (+). Additionally, APPI (+) enabled the potential identification of HMT-$NH_2$ ($C_6H_{13}N_5$) and HMT-CHO ($C_7H_{12}N_4O$), increasing the total potential HMT-related assignments. APPI (+) appears to be less efficient than ESI (+) in detecting high-mass CHN species.

A limited number of CH compounds were detected in the SOMA-1 organic residue using APPI (+): $C_{10}H_{14}$, $C_{10}H_{16}$, $C_{11}H_{18}$, $C_{13}H_{20}$, with an average DBE and $X_c$ of 4 and 2.42 respectively, an average ion mass of $m/z$ 150.14029 and an H/C ratio of 1.54. Further experiments are necessary to conclude on the detection of CH compounds after methanol extraction in the SOMA fraction. Nevertheless, these preliminary results offer first insights into the possible distribution of the CH group, with the most volatile species being observed in the gas-phase analyses of similar analogues (T. Javelle et al. 2025).

Although APPI (+) ionization mode appears to be less sensitive than ESI in terms of intensities and total number of molecular formulas detected, it none the less provided additional unique assignments, thereby significantly contributing to the molecular characterization of the sample. Notably, a higher number of scans and longer ion accumulation times were applied during APPI (+) acquisition compared to ESI (+), partially compensating for its lower sensitivity.

### 3.4. APPI (−) FT-ICR MS analysis

APPI (−) analyses were performed exclusively on the SOMA-1 sample. APPI in negative mode involves ionization processes leading to the formation of both deprotonated compound $[M-H]^-$ and radical anions $[M]^{\bullet-}$, which represent 99 per cent and 1 per cent of the total assignments, respectively. The 19 compounds detected as radical anions exhibit characteristics of short ($m/z$ 261.97128) saturated compounds (H/C = 1.88) with high degree of oxidation (O/C = 0.47), a high content in nitrogen (N/C = 0.56) and bearing few unsaturations (DBE = 4 and $X_c$ = 1.34). Previous studies have investigated the APPI (−) ionization processes and demonstrated the possibility for organic compounds to form stable radical anions if they present positive electron affinity (EA), specifically cyclic and aromatic compounds, through electrophilic functional groups, such as -$NO_2$ nitro group, for example (L. Song et al. 2007, 2009; C. N. McEwen & B. S. Larsen 2009). However, they also demonstrated the role of $O_2$, as an intermediate in the form of $[M + O_2]^{\bullet-}$, and in the formation of $[M-H]^-$ ions via proton transfer. Since this reaction is reversible, the presence of $[M + O_2]^{\bullet-}$ is also very likely. Indeed, 16 molecular formulas corresponding to $[M]^{\bullet-}$ were also observed as a ($[M]^{\bullet-}$- $O_2$) within the $[M-H]^-$ ion population. For example, the formula $C_9H_{18}N_4O_4$ was also detected as $C_9H_{18}N_4O_2$ in the $[M-H]^-$ data set. These observations suggest that most of the detected radical anions are likely $[M + O_2]^{\bullet-}$ species than $[M]^{\bullet-}$ radicals.

Among the four ionization modes used in this study, APPI (−) proved to be the least descriptive for this sample. A total of 2165 molecular formulas were assigned, essentially related to CHNO class. Elemental ratios revealed unique characteristics with average H/C, O/C, and N/C ratios of 1.60, 0.39, and 0.39, respectively, showing a higher heteroatom content than compounds detected using positive ion mode APPI. These findings are consistent with a predominance of oxygenated alkyl chains, as evidenced by the large proportion of category 2b (43 per cent – Fig. 1b), followed by categories 2a (20 per cent) and 2c (7 per cent). As in APPI (+), the proportion of category 3b reaches 27 per cent, highlighting the enhanced sensitivity of photoionization towards oxygenated conjugated structures.

The majority of formulas (52 per cent) display an $X_c$ below 2.5 and are thus classified as aliphatic compounds. Among them, 882 assignments (41 per cent) fall within the $X_c$ range of 1–2.5, with a slight increase of the hydrogen amount (H/C = 1.69) and oxygen content (O/C = 0.45). In contrast with APPI (+) distribution, these species contain a significant number of heteroatoms. Compounds with low aromaticity ($X_c$ < 1; 234 formulas – 11 per cent) exhibit higher hydrogen amount (H/C = 1.90), elevated oxygen content (O/C = 0.67) and a lower nitrogen incorporation (N/C = 0.29). A low aromaticity is thus characterized by an increase of the oxidation degree and a nitrogen depletion, as observed among the four ionization modes. This subset likely includes saturated short-chain compounds ($m/z$ 268.43666) containing multiple unsaturated or acidic functional group such as hydroxyl group, amide, ether, amino acids, or carboxylic acids.

Aromatic molecules account for 1049 molecular formulas (48 per cent) and present an average DBE of 7. This subset is characterized by higher mass features ($m/z$ 335.52498), with a lower hydrogen content (H/C = 1.46), and a reduced oxygen incorporation (O/C = 0.28). These results demonstrate the sensitivity of APPI (−) towards conjugated structures, likely with phenyl groups, a significant nitrogen incorporation and few unsaturated oxygenated functional groups.

## 4. DISCUSSION

### 4.1. Advantages and limitations of the ionization modes

A comparative analysis of the molecular formulas for SOMA-1 obtained from each ionization mode was performed using a Venn diagram (Fig. 3). Detected adducts such as $Cl^-$, $Na^+$, and $K^+$ were excluded from the molecular formulas to only compare neutral form, and duplicate assignments were removed. This representation highlights both the complementarity and distinctiveness of the different ionization modes. In total, 15 unique subsets were identified, corresponding to assignments detected by only one or by combinations of multiple ionization modes. Overall, 14 889 raw formulas were assigned as unique attributions, including 12 per cent (1855) that were detected exclusively by using APPI (+) mode, and 0.4 per cent (60) by using APPI (−) mode, providing additional information on the molecular diversity, thereby significantly contributing to the molecular characterization of this sample.

Our study highlights the importance of adopting a multimodal ionization approach for maximizing the molecular information obtained from SOMA. ESI in positive mode proves to be the most informative mode, ionizing the widest molecular diversity in this sample. Considering all subset of the Venn diagram, ESI (+) alone covers 60 per cent of the 14 889 molecular formulas detected. These include a majority of CHNO molecules, rich in heteroatoms, specifically nitrogen, and span from aliphatic to aromatics structures. ESI (+) shows high sensitivity towards basic compounds, providing a global view on the nature of the residue, largely characterized by two molecular distributions: (1) unsaturated species containing aromatic moieties, heterocycles, ether, amide, ester or imine functionalities, and (2) more saturated species bearing hydroxyl, carboxyl, or amine groups.

ESI in negative-ion mode is essential to access oxygen-rich and aliphatic compounds. Fig. 1 illustrates its specific sensitivity to hydrogen-saturated alkyl chain with high O/C and H/C ratio, including the most acidic species in the residue. The negative-ion mode also plays a crucial role in probing the CHO molecular class, including fatty-acids-like structures, carbohydrates, and polyols. Overall, 1079 CHO formulas were detected across all ionization modes, with ESI (−) covering 64 per cent (692) (Fig. 3), and exclusively detecting 27 per cent (292) of them (see Fig. S5 in Supporting Information). ESI (−) predominantly targets aliphatic structures with low $X_c$ values.

APPI distinguishes itself by efficiently ionizing low-mass, heteroatom-poor, and aromatic molecules (H. Keski-Hynnilä et al. 2002; K. A. Hanold et al. 2004; S.-S. Cai & J. A. Syage, 2006). APPI (+) revealed additional molecular diversity across all chemical classes composing the residue (see Fig. S5 in Supporting Information). This ionization mode exhibits particular sensitivity toward CHO species, detecting 32 per cent (342) new molecular formulas compared to ESI, with higher unsaturation and lower oxidation states. It also revealed 22 per cent (67) previously undetected highly aromatic CHN structures. These findings provide new insights into the composition of the residue, suggesting the presence of compounds likely composed of N- or O-bearing heterocycles, and unsaturated oxygen-bearing functionalities such as

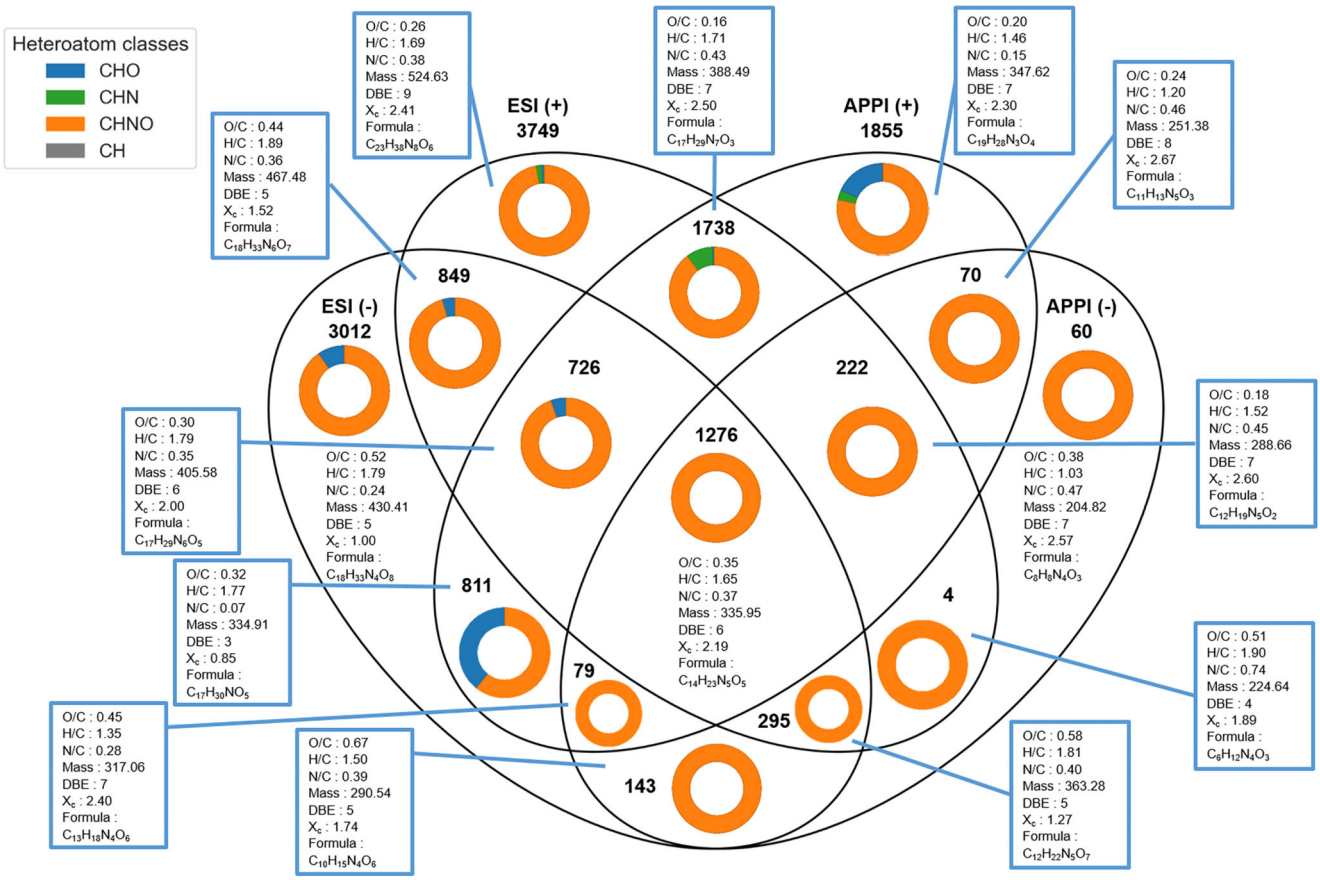


**Figure 3.** Venn diagram achieved from data obtained in ESI- and APPI-FT-ICR MS in both positive- and negative-ion modes, from SOMA-1 organic residue made from VUV irradiated interstellar ice analogues. Each ellipse represents one ionization mode used in this study. The intersections between ellipses correspond to molecular formulas detected by two, three, or all four analytical conditions. For example, the central overlapping area represents 1276 molecular formulas that were detected with all four analytical conditions, defining a shared population common to the four ionization modes. Molecular formulas detected by multiple ionization modes may correspond to several distinct isomers. The displayed values represent the averages of each distribution, taking into account all heteroatom classes. For the mean values of each class, see Figs S5 and S6 in Supporting Information.

carbonyl or amide groups, as well as nitrogen-bearing chemical function such as imines or nitriles. Notably, APPI (+) was the only mode able to detect CH-only compounds, although only in limited numbers, suggesting a possible depletion of this chemical class in the sample due to a release of the most volatile hydrocarbons in the gas phase during the warming process of the ice (T. Javelle et al. 2025).

In contrast, APPI (−) mode detected only 60 additional CHNO molecular formulas. Nevertheless, it revealed a notable molecular diversity, including short aromatics structures enriched in nitrogen and oxygen atoms. These species were predominantly detected as deprotonated ions and may correspond to nitrogen-rich acidic compounds, such as hydroxylated pyridine derivatives or carboxylic acids covalently bound to N-heterocycle moieties. Other structures, including aromatic imides, hydrazides, and semicarbazides, likely detected in ESI (−) ionization mode, may also contribute for such molecular diversity. While APPI (−) appears valuable for targeting specific chemical families, it remains limited in providing a comprehensive molecular overview of our sample.

It is worth noting that the subsets involving formulas detected by different ionization modes [e.g. APPI (+) – ESI (−), or ESI (+) – ESI (−)], based on distinct ionization process and efficiency, indicate that multiple isomers of a given molecular formulas are likely present in the residue. These observations further expand the apparent molecular diversity of the sample.

### 4.2. Improvements over prior research works

The overall distribution of the SOMA-1 sample in the present study exhibits the following average characteristics: H/C = 1.68; O/C = 0.33; N/C = 0.31; $m/z$ 419.76046; formula = $C_{19}H_{31}N_5O_5$; DBE = 7; and $X_c$ = 1.93. The CHNO group represents the largest class of compounds, accounting for 91 per cent of the assignments, followed by CHO with 7 per cent of the molecular formulas, CHN compounds with 2 per cent, and finally CH representing 0.03 per cent.

These values are slightly different from those reported by G. Danger et al. (2016), where H/C = 1.80; O/C = 0.50; and N/C = 0.2 were observed with similar residues analysed using ESI (±) Orbitrap-MS, with a total of 2529 assignments on the $m/z$ 50–400 range. In comparison, 5533 unique molecular formulas were detected in this work under the same mass parameters (considering only ESI features), corresponding to an improvement by approximately a factor of two. The average values of the molecular diversity detected in these parameters are therefore slightly different, with elemental ratio such as H/C = 1.71, O/C

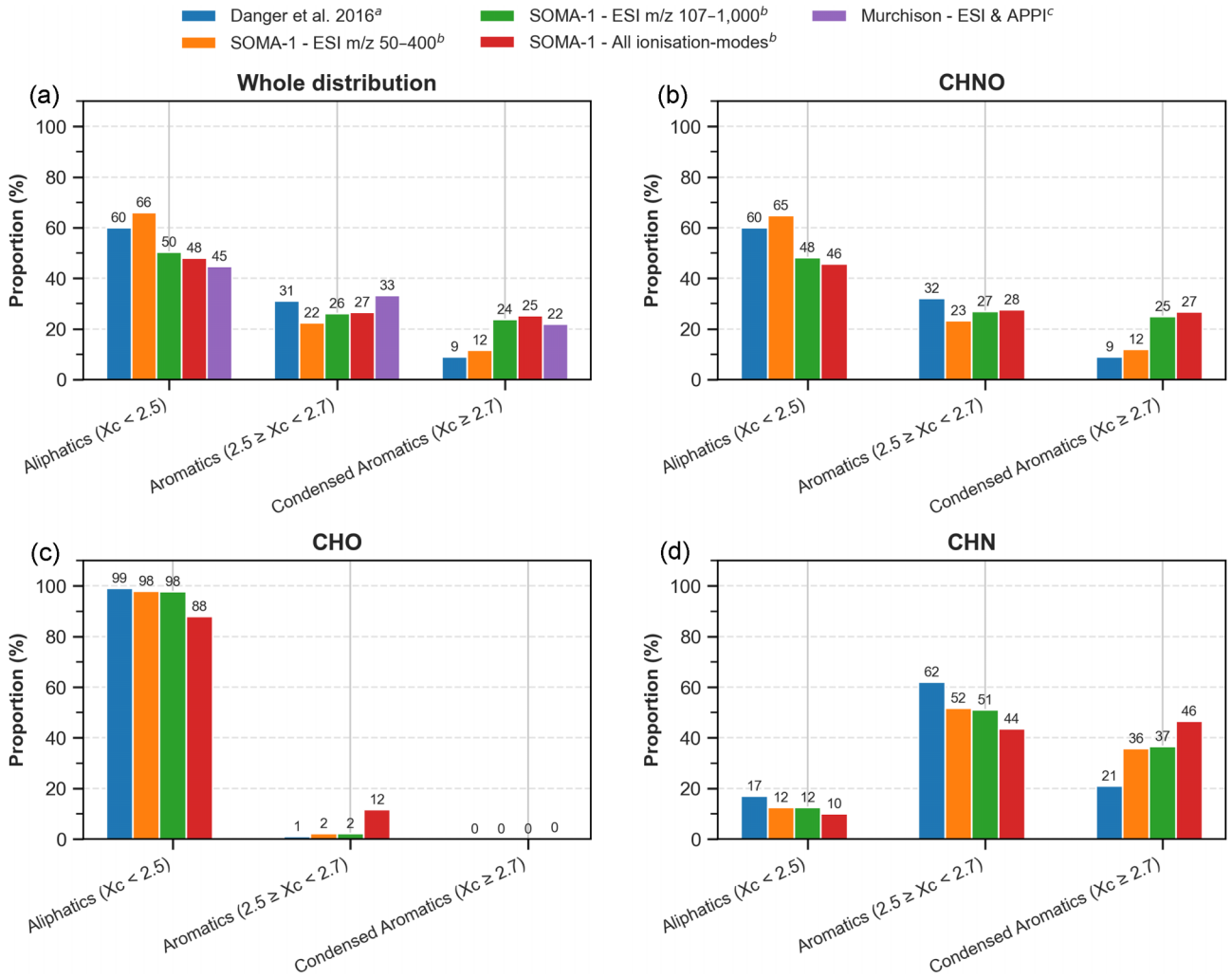


**Figure 4.** Aromaticity distribution of SOMA-1 based on the aromaticity equivalent parameter $X_c$ from M. M. Yassine et al. (2014). Molecular formulas with $0 \leq X_c < 2.5$ are categorized as aliphatics; compounds with $2.5 \leq X_c < 2.7$ are considered as aromatic; assignments with an $X_c$ index higher or equal to 2.7 are classified as condensed aromatic. (a) Data extracted from G. Danger et al. (2016), obtained with ESI-Orbitrap-MS in the mass range $m/z$ 50–400. (b) Data from this work. (c) Data extracted from J. Hertzog et al. (2019).

= 0.40, and N/C = 0.30. It must be noted that the lower mass limit during our analyses was set at $m/z$ 107.5, likely losing a part of the information on the low-molecular weight compounds. An additional comparison can be made with the results of G. Danger et al. (2021), where 3964 molecular formulas were identified in a similar residue using ESI-FT-ICR MS over the mass range from $m/z$ 147 to 1000. In this work, 12 904 molecular formulas were detected under a similar mass range, representing an approximately threefold improvement in molecular coverage. This enhancement likely results from differences in the FT-ICR MS setup. The reported average elemental ratios were 1.67, 0.39, and 0.22 for H/C, O/C, and N/C respectively, with an average DBE of 6, which are closer to our results, despite a slight depletion in nitrogen. The 2xR technology implemented in the FT-ICR MS used in this study provides enhanced sensitivity and signal amplification, enabling the detection of higher mass species up to $m/z$ 850 and a broader molecular diversity, thereby allowing a more accurate characterization of the sample. ESI, particularly in positive mode, remains the most exhaustive mode across the overall molecular distribution of our sample. None the less, these results highlight the importance of the instrumental configuration, which can significantly influence the data obtained from similar sample, by revealing different facets of the molecular diversity, notably through enhanced sensitivity. The higher is the number of distinct compounds detected, the more accurate the information obtained about the sample, and ultimately, the better our understanding of its chemical evolution. This is further illustrated by the use of complementary ionization modes that significantly enhances the chemical coverage, by revealing additional molecular diversity, which remained undetected using only ESI, and allowing access to a broader range of compound classes.

Regarding the aromaticity class distributions (Fig. 4a), the ESI data within the $m/z$ 50–400 range show values comparable to those reported by G. Danger et al. (2016), who used Orbitrap-MS analyses in the same mass range. A slightly higher proportion of aliphatic compounds is observed across the overall distribution in their study. A stronger representation of the condensed aromatics is also noted, specifically in the CHN class with an increase up to 36 per cent. These results are likely attributable to differ-

**Table 2** Description of the SOM of the Murchison meteorite, adapted from J. Hertzog et al. (2019), analysed by ESI-FT-ICR MS in positive and negative modes, and APPI in positive mode. Number of assignments detected for each class of molecules (CH, CHO, CHONa, CHOS, CHN, CHON, CHONS, and CHOMg), percentages of atomic ratios, as well as the average DBE, $X_c$, mass, and formula of each mass list are displayed.

| Heteroatom class | ESI (−) | ESI (+) | APPI (+) |
|---|---|---|---|
| CH | 12 (0.1 per cent) | 4 (0.1 per cent) | 402 (9.2 per cent) |
| CHO | 1530 (13.3 per cent) | 6 (0.1 per cent) | 1368 (31.4 per cent) |
| CHONa | – | 285 (6.4 per cent) | – |
| CHOS | 2544 (22.0 per cent) | 3 (0.1 per cent) | 286 (6.5 per cent) |
| CHN | 150 (1.3 per cent) | 747 (16.8 per cent) | 421 (9.7 per cent) |
| CHNO | 3544 (30.7 per cent) | 2104 (47.2 per cent) | 1685 (38.6 per cent) |
| CHNOS | 3618 (31.3 per cent) | 524 (11.8 per cent) | 198 (4.5 per cent) |
| CHOMg | 151 (1.3 per cent) | 786 (17.6 per cent) | – |
| Total assigned features | 11 549 | 4459 | 4360 |
| Average O/C | 0.24 | 0.13 | 0.09 |
| Average H/C | 1.41 | 1.69 | 1.56 |
| Average N/C | 0.05 | 0.06 | 0.02 |
| Average DBE | 8 | 7 | 7 |
| Average $X_c$ | 2.11 | 2.01 | 2.20 |
| Average mass | 391.02 842 | 436.60 260 | 355.72 429 |
| Average formula | $C_{20}H_{29}NO_4$ | $C_{25}H_{43}N_2O_3$ | $C_{23}H_{36}NO_2$ |

ences in the analytical setup used, revealing higher proportion of these aromatic species. When considering the results obtained using the multimodal ionization analyses within the full mass range ($m/z$ 107.5–1 000), the data revealed a significant increase in aromatic and condensed aromatic compounds highlighting a correlation between molecular aromaticity and mass, especially due to the contribution of APPI on these categories of molecules. In particular, for CHO compounds, the use of ESI ionization alone led predominantly to the detection of aliphatic and polar molecules, thereby missing the aromatic CHO diversity that is revealed when using APPI (+) ionization mode.

Finally, the analyses of multiple samples, differing by slight variations in their initial ice composition, allowed us to investigate the variability of the molecular diversity generated in our experiments. As discussed in Section 2.3.1. the instrumental variability itself is too low to account for the molecular diversity differences observed, confirming that these variations arise from compositional differences in the initial ice mixtures of each sample. A figure illustrating the variability in the molecular formula distributions among the three samples is provided in Supporting Information (see Fig. S4). Considering the proportion of molecular formulas only detected in one sample as an indicator of variability, we found that the average molecular diversity variability across this study was about ± 11 per cent. This limited level of variability indicated that the molecular diversity produced under our experimental conditions is largely reproducible and robust with respect to small variations in the initial ice composition. The majority of molecular formulas (89 per cent) are consistently detected across the different samples, suggesting that the dominant chemical formation pathways are not strongly affected by minor changes in the relative abundances of the ice constituents, even though large variations in ice composition can significantly impact the nature of the organic matter formed (A. Fresneau et al. 2017). This reinforces the reliability of the experimental approach and supports the relevance of these results for interpreting the chemistry of VUV-processed interstellar ice analogues. In another approach, the use of different irradiation sources may lead to variations in organic diversity (P. A. Gerakines, M. H. Moore & R. L. Hudson 2001; M. H. Moore, R. L. Hudson & P. A. Gerakines 2001; G. M. Muñoz Caro et al. 2014), as well as in relative abundances (B. L. Henderson & M. S. Gudipati 2015). Such experiments would help to better understand the differences arising from chemical composition of the ices and from the experimental parameter employed, such as the irradiation source. In this study, however, we specifically focus on the impact of VUV irradiation on icy analogues.

## 5. COMPARISON WITH MURCHISON METEORITE

The recent work of M. Bizzarro et al. (2025) on meteorites suggests that the earliest parent bodies of interplanetary objects accreted significant amount of interstellar ices and likely primitive organic matter originating from the dense molecular cloud. This supports the hypothesis that the organic matter found in meteorites may originate from molecular clouds environments, and subsequently evolved within interplanetary bodies, notably through aqueous alteration processes. It is therefore interesting to compare our analogues, detailed using advanced analytical techniques and protocols, to organic composition of natural samples.

A detailed comparative assessment was undertaken using data from J. Hertzog et al. (2019), which were reprocessed to allow for direct comparison with the results of this study (Table 2). We specifically focused on CH, CHO, CHN, and CHNO molecules, as neither sulphur nor magnesium were introduced in the initial composition of the ice analogue. Considering these compounds classes, the Murchison meteorite exhibits non-weighted average molecular characteristics such as: H/C = 1.52; O/C = 0.17; N/C = 0.06; DBE = 8; $X_c$ = 2.15; $m/z$ 407.38774; and formula = $C_{23}H_{36}N_2O_3$.

In this work, the use of FT-ICR MS allowed a more direct comparison of the results obtained from the residue with those of the meteorite, in contrast to G. Danger et al. (2016), who conducted Orbitrap-MS analyses and consequently detected a more limited molecular diversity. Moreover, by using a different analytical system and a multimodal ionization approach, the molecular coverage is significant enhanced compared to G. Danger et al. (2021), providing more comprehensive molecular information for comparing the simulated pristine SOMA with natural extraterrestrial samples.

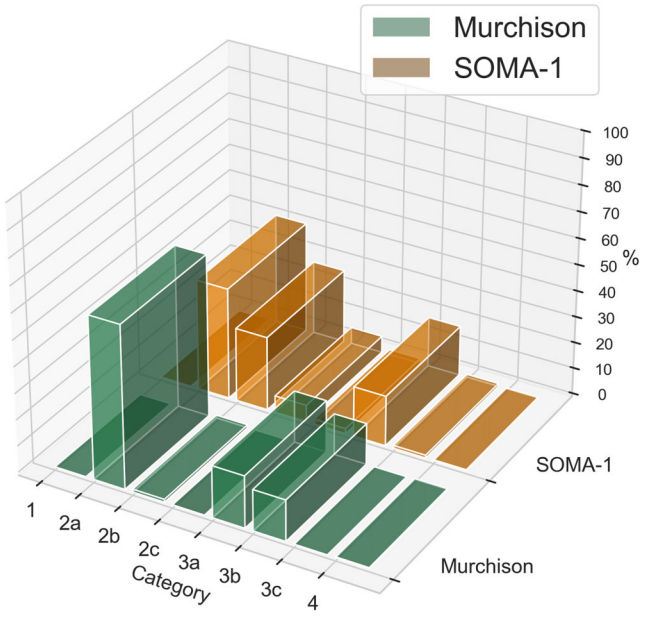


**Figure 5.** Comparison of the van Krevelen categories distributions of Murchison meteorite and SOMA-1 sample, based on G. Danger et al. (2016) partitions. Results are not weighted by the intensities to avoid biases from ionization mechanisms of each mode, difference through scan numbers and ion accumulation times used. Category 1: fully saturated structures -OR/-$NR_1R_2$. Category 2a: alkyl chains with $CO_2H$/$CONH_2$. Category 2b: alkyl chains (-$CO_2$R)n/(-$CONR_1R_2$)n/-$NR_1R_2$. Category 2c: alkyl chains enriched in O (-$CO_2$R)n/-OR with low amount of N. Category 3a: conjugated structures with possible phenyl groups enriched in N with few O functions. Category 3b: conjugated structures with possible phenyl groups (-$CO_2$R)n/(-$CONR_1R_2$)n/-$NR_1R_2$. Category 3c: conjugated structures with possible phenyl groups, enriched in O with few N functions. Category 4: highly aromatic structures with O and N functions.

A significant depletion in nitrogen is observed, with N/C ratio decreasing from 0.31 in the SOMA to 0.06 in Murchison's SOM. A concurrent loss of oxygen is also evident, with the O/C ratio halved from 0.33 to 0.17. This reduction is further reflected in the predominance of the less oxygenated van Krevelen classes (2a and 3a) (Fig. 5). A slight decrease in hydrogen content may be linked to an increase in unsaturation and aromaticity, as shown by elevated DBE and $X_c$ values. Structurally, this evolution corresponds to molecules with longer carbon chains, more unsaturated, and depleted in heteroatoms. Previous experiments tentatively explored the evolution of residue in interplanetary object conditions, by simulating the effects of aqueous alteration on the molecular diversity of organic residue produced from interstellar ice analogues (G. Danger et al. 2021). Notably, they demonstrated that such alteration processes, likely occurring in parent bodies of meteorites, can lead to a depletion in heteroatoms within the soluble organic matter (SOM) from residues, particularly nitrogen, while enhancing the degree of unsaturation in the carbon backbone.

In Murchison, CHNO compounds remain the dominant class, with a notable increase of the proportion of CHO molecules, particularly in APPI (+), where more than 30 per cent of the total assignments of molecular formulas correspond to CHO species. A prevalence of low-oxidized CHO compounds is observed with the $O_1$, $O_2$, and $O_3$ groups accounting for 77 per cent of the CHO species detected using APPI (+) ionization mode. These compounds exhibit high unsaturation and aromaticity (DBE = 7 and $X_c$ = 2.05), indicating the predominance of aromatic and unsaturated, low-oxidized CHO structures, consistent with the general increase in unsaturation observed.

CHN compounds are more abundant in the Murchison meteorite, with a higher number of assigned molecular formulas and higher average ion masses compared to the residue, reaching *m/z* 335.21920 and 413.99440 for APPI (+) and ESI (+) modes, respectively. In APPI (+), the detected species exhibit a marked decrease in N/C ratio down to 0.04, corresponding to an average of two nitrogen atoms per formula. A reduction in the aromaticity index ($X_c$ = 2.34) is also observed, likely associated with nitrogen loss, as well as an increase in the H/C ratio (H/C = 1.69). This suggests a higher proportion of aliphatic or unsaturated alkyl structures at the expense of the N-heterocycles detected in the residue. The unsaturation likely arises on these compounds from conjugated systems, such as phenyl groups or C = C double bonds, rather than being driven by nitrogen-containing aromatic rings. Similar trends are observed in ESI (+) mode, where the detected CHN compounds display slightly lower average aromaticity ($X_c$ = 2.43) and a clear depletion in nitrogen content (N/C = 0.06), also with exhibiting an average of two nitrogen atoms per formula. Altogether, these results suggest a general decrease of the aromatic class for CHN molecular formulas.

Concerning CH compounds, only four compounds were observed in our sample. In comparison, J. Hertzog et al. (2019) reported 402 CH assignments in Murchison meteorites using APPI (+) with a different analytical setup. These compounds showed an average of *m/z* 340.31470 ion with average DBE and $X_c$ of 7 and 2.63, respectively, and an H/C ratio of 1.50. Despite some similarities, such as high $X_c$ values and comparable H/C ratios, the limited number of CH species detected in this work prevents robust statistical comparisons. Additionally, 45 per cent of the CH compounds detected in Murchison meteorite were in radical cation form, absent from our results. A greater number of CH-compounds were detected in the SOMA-3 sample (see Table S5 in Supporting Information), with 27 molecular formulas assigned, further confirming the very low abundance of such species in organic residue made from the experimental conditions used in this study.

It should be noted that, ESI (+) analyses of residue yielded the highest number of unique molecular formulas, whereas in the Murchison meteorite, ESI (−) proved to be the most informative ionization mode. This difference may reflect the relative enrichment in CHO species, consistent with aqueous alteration processes previously observed in interstellar ice residues (G. Danger et al. 2021). Compounds detected via ESI (−) exhibit higher aromaticity than organic diversity detected from residues. Aliphatic molecules such as polyols are no longer present in the meteorite, with CHO formulas exhibiting reduced H/C ratios (1.47) and higher unsaturation degree (DBE = 7), consistent with increased aromaticity. As a results, the molecular composition of Murchison meteorite is dominated by three categories (Fig. 5): long alkyl chains with low heteroatom content (2a; 62.0 per cent), low-oxidized aromatics (3a; 19.8 per cent), and moderately oxidized aromatics (3b; 15.7 per cent). In contrast to interstellar ice analogues, where category 3b is the predominant group among the most unsaturated species, the present results suggest a comparatively lower oxidation state in conjugated structures.

Overall, Murchison meteorite shares only about 7 per cent of its molecular diversity with organic residues from VUV-processed ice analogues. Notably, despite the enhanced molecular cover-

age achieved in this work, we reached the same conclusions as G. Danger et al. (2021): organic matter derived solely from ice analogues subjected to energetic processing appears to be very distinct from the SOM of the meteorite. This highlights the necessity of using altered analogues to simulate the various processing pathways that likely occurred within meteorite parent bodies, which significantly influenced their molecular diversity. In particular, aqueous alteration appears to increase aromaticity and deplete the SOMA of heteroatoms, likely leading to the formation of new unsaturated chemical species that remain undetectable using only ESI (G. Danger et al. 2021). Therefore, it is essential to apply similar analytical protocols and sensitivities when probing the SOMA of aqueously altered analogues to enable more accurate comparisons with meteorite and natural samples. Furthermore, the molecular composition of such analogues may be influenced by multiple factors prior to post-accretion alteration processes. These include: the initial ice composition, which can affect chemical reactions occurring both in the desorbing gas phase (N. Abou Mrad et al. 2017; T. Javelle et al. 2025) and in the solid phase (R. Briggs et al. 1992; P. A. Gerakines et al. 2001; G. M. Muñoz Caro & W. A Schutte, 2003; J. P. Dworkin et al. 2004; Y. Takano et al. 2004; M. Nuevo et al. 2007; Y.-J. Chen et al. 2011; R. Hodyss et al. 2011; C. K. Materese et al. 2015; A. Fresneau et al. 2017; T. Gautier et al. 2020; R. L. James et al. 2021; A. Ruf & G. Danger, 2022); the type of irradiation simulated (G. Strazzulla et al. 1995; P. A. Gerakine et al. 2001; M. H. Moore et al. 2001; F. Islam, G. A. Baratta & M. E. Palumbo 2014; G. M. Muñoz Caro et al. 2014; B. L. Henderson & M. S. Gudipati 2015; P. De Marcellus et al. 2017; R. L. Hudson & M. H. Moore 2018; R. G. Urso et al. 2020, 2022), which influences both the molecular diversity and the relative abundance of products; thermal processes, which can generate molecular diversity even in absence of energetic processing (J. B. Bossa et al. 2008; V. Vinogradoff et al. 2011; P. Theulé et al. 2013; G. Danger et al. 2014; A. Fresneau et al. 2014; Y. Rodríguez-Lazcano et al. 2014; G. Fedoseev et al. 2015) and modify the chemical properties of the residue (A. Garcia et al. 2024).

## 6. CONCLUSION

In this study, we report, for the first time, the application of a multimodal ionization approach, combining ESI and APPI, for non-targeted FT-ICR MS analysis of organic residues derived from interstellar ice analogues composed of $H_2O$-$CH_3OH$-$NH_3$ mixtures.

APPI is widely acknowledged as an ionization mode particularly suited for the detection of mid- to non-polar species, with a strong affinity for aromatic compounds. By combining complementary ionization and detection modes, APPI (+), APPI (−), ESI (+), and ESI (−), we achieved a broad range of organic molecules, revealing nearly 15 000 unique molecular formulas and providing new insights into the chemical diversity of organic residues from VUV-processed interstellar ice analogues by significantly improving the molecular coverage of these samples. Notably, we increased the number of distinct molecular formulas detected by approximately a factor of three compared to previous work, and 12 per cent of these molecular formulas are newly detected, having not been observed in prior studies on similar samples without the use of APPI. It should be noted that a single chemical formula can correspond to multiple isomers, as the ionization efficiency of these different isomers likely varies across the mode used. Undoubtedly, this data set highlights more than 15 000 distinct compounds, underscoring the immense potential molecular diversity formed in star-forming regions and likely incorporated into the parent bodies of interplanetary objects through accretion processes.

Electrospray, in both polarities, proved to be the most descriptive mode for such sample, accounting for over 51 per cent of the total molecular diversity, and up to 87 per cent when including formulas shared with APPI. Notably, APPI (+) enabled the detection of a distinct set of organic molecules not observed in previous work, that were either poorly ionized or not detected by ESI. These include unsaturated CHO species depleted in oxygen and highly condensed aromatic CHN compounds exhibiting signals characteristics of N-heterocycles. APPI (+) also highlights the very low abundance of CH hydrocarbons in the samples. APPI in negative mode proved to be not informative for characterizing the SOMA of organic residues, although this mode may still be valuable for targeting specific chemical features, such as polar chromophore-containing species.

Based on the combined data set from the four analytical conditions, average elemental ratios and molecular characteristics were calculated: H/C = 1.68; O/C = 0.33; N/C = 0.31; *m/z* 419.76046; formula = $C_{19}H_{31}N_5O_5$; DBE = 7; and $X_c$ = 1.93. Analyses of samples prepared from similar, though slightly different, initial ice mixtures revealed the low variability of such experiments, with only about 11 per cent of the molecular formulas being unique to each sample. These average values underscore the polar nature of residues from VUV-processed interstellar ice analogues, with a prevalence of heteroatom-rich species featuring multiple unsaturations in their carbon backbones. CHNO molecular group still dominates the distribution, followed by CHO, CHN, and finally CH-group in only limited proportions. Regarding structural classification, the samples are mainly composed of aliphatic alkyls chains with low heteroatoms content, followed by more oxidized alkyl structures and conjugated systems with moderate oxidation degree. APPI specifically contributed to the characterization of this latter group. These findings are then consistent with previous HRMS studies on interstellar ice analogues, which have shown a limited correlation with the SOM observed in meteorites, with higher heteroatom content and lower average unsaturations.

This multimodal ionization approach enhances our ability to probe the chemical complexity organics generated from the energetic processing of astrophysical ices. It demonstrates the analytical relevance of combining APPI and ESI to achieve a more comprehensive view of molecular diversity in laboratory analogues, contributing valuable insights into the chemical evolution of organics within the early Solar system.

## ACKNOWLEDGEMENTS

The research was funded by the Centre National d'Etudes Spatiales (CNES, R-S18/SU-0003–072 and R-S18/SU-0003–072, PI: GD), and the Centre National de la Recherche Scientifique (CNRS) with the program 'Physique et Chimie du Milieu Interstellaire' (PCMI-PI: GD) and 'Programme National de Planétologie' (PNP) (PI: GD). GD is grateful to the Agence Nationale de la Recherche for funding via the ANR RAHIIA_SSOM (ANR-16-CE29-0015) and VAHIIA (ANR-12-JS08-0001). The project has further received funding from the EXCellence Initiative of Aix-Marseille Université – A∗Midex, a French 'Investissements d'Avenir programme' AMX-21-IET-018, Université – A∗MIDEX AMX-21-PEP-032, and from the Région SUD Provence Alpes Côte d'Azur 'Apog 2017' – PILSE. Funded by the Deutsche Forschungs-

gemeinschaft (DFG, German Research Foundation) under Germany's Excellence Strategy – EXC 2094–390783311 (AR). Financial support from the IR INFRANALYTICS FR2054 for conducting the research is gratefully acknowledged. This work was partially supported by the MassLor research infrastructure at the University of Lorraine. This work was supported by the French National Research Agency under France 2030 investment plan (reference ANR-22-EXOR-0012, project MIRRPLA, PI: AD). LH acknowledge support from Institute Origins Marseille and France 2030 investment plan (project MIRRPLA).

## DATA AVAILABILITY

The data underlying this article will be shared on reasonable request to the corresponding author.

## REFERENCES

Abou Mrad N. et al. 2016, MNRAS, 458, 1234
Abou Mrad N. et al. 2017, ApJ, 846,124
Agarwal V. K. et al. 1985, Orig. Life Evol. Biosph., 16, 21
Aponte J. C. et al. 2023, Earth Planets Space, 75, 28
Bernstein M. P. et al. 1995, ApJ, 454, 327
Bernstein M. P. et al. 2002, Nature, 416, 401
Bizzarro M. et al. 2025, Nat. Commun., 16, 10657
Boogert A. C. A. et al. 2022, ApJ, 941, 32
Boogert A. C. A., Gerakines P. A., Whittet D. C. B. 2015, ARA&A, 53, 541
Bossa J. B. et al. 2008, A&A, 492, 719
Bouilloud M. et al. 2015, MNRAS, 451, 2145
Bouquet A. et al. 2024, Planet. Sci. J., 5, 102
Briggs R. et al. 1992, Orig. Life Evol. Biosph., 22, 287
Cai S.-S., Syage J. A. 2006, J. Chromatogr. A, 1110, 15
Chen Y.-J. et al. 2011, Adv. Space Res., 47, 1633
Cottin H., Moore M. H., Benilan Y. 2003, ApJ, 590, 874
Cruz-Diaz G. A. et al. 2014, A&A, 562, A119
Cuppen H. M., Linnartz H., Ioppolo S. 2024, ARA&A, 62, 243
Danger G. et al. 2011, A&A, 525, A30
Danger G. et al. 2013, Geochim. Cosmochim. Acta, 118, 184
Danger G. et al. 2014, Phys. Chem. Chem. Phys., 16, 3360
Danger G. et al. 2016, Geochim. Cosmochim. Acta, 189, 184
Danger G. et al. 2021, Nat. Commun., 12 3538
Danger G. et al. 2022, A&A, 667, A120
Del Burgo Olivares C. et al. 2025, A&A, 698, A285
De Marcellus P. et al. 2011, ApJ, 727, L27
De Marcellus P. et al. 2015, Proc. Natl. Acad. Sci., 112, 965
De Marcellus P. et al. 2017, MNRAS, 464, 114
d'Hendecourt L. L. S. et al. 1982, A&A, 109, 12–14
Dworkin J. P. et al. 2004, Adv. Space Res., 33, 67
Elsila J. E. et al. 2007, ApJ, 660, 911
Endres C. P. et al. 2016, J. Mol. Spectrosc., 327, 95
Fedoseev G. et al. 2015, MNRAS, 448, 1288
Fresneau A. et al. 2014, MNRAS, 443, 2991
Fresneau A. et al. 2017, ApJ, 837, 168
Furukawa Y. et al. 2025, Nat. Geosci., 19, 19–24
Garcia A. 2023, La chromatographie gazeuse couplée à de la spectrométrie de masse Orbitrap comme analyseur de matière organique pour des futures missions spatiales [Doctoral dissertation, PIIM Laboratory, Aix-Marseille University, France], https://theses.fr/2023AIXM0544, 242
Garcia A. et al. 2023, J. Chromatogr. A,1704, 464118
Garcia A. et al. 2024, ACS Earth Space Chem., 8, 606
Gaspar A. et al. 2012, Anal. Chem., 84, 5257
Gautier T. et al. 2020, Earth Planet. Sci. Lett., 531, 116011
Gerakines P. A., Moore M. H., Hudson R. L. 2001, J. Geophys. Res. Planets, 106, 33381
Glavin D. P. et al. 2025, Nat. Astron., 9, 199
Hanold K. A. et al. 2004, Anal. Chem., 76, 2842
Henderson B. L., Gudipati M. S. 2015, ApJ, 800, 66
Hertkorn N. et al. 2008, Anal. Chem., 80, 8908
Hertkorn N., Harir M., Schmitt-Kopplin P. 2015, Magn. Reson. Chem., 53, 754
Hertzog J. et al. 2017, Anal. Chim. Acta, 969, 26
Hertzog J., Naraoka H., Schmitt-Kopplin P. 2019, Life, 9, 48
Hockaday W. C. et al. 2009, Limnol. Oceanogr.: Methods, 7, 81
Hodyss R. et al. 2011, Icarus, 214, 748
Huba A. K., Huba K., Gardinali P. R. 2016, Sci. Total Environ., 568, 1018
Hudson R. L., Moore M. H. 2018, ApJ, 857, 89
Islam F., Baratta G. A., Palumbo M. E. 2014, A&A, 561, A73
James R. L. et al. 2021, RSC Adv., 11, 33055
Javelle T. et al. 2024, MNRAS, 534, 2305
Javelle T. et al. 2025, Commun. Chem., 8, 306
Kebarle P., Tang L. 1993, Anal. Chem., 65, 972A
Keski-Hynnilä H. et al. 2002, Anal. Chem., 74, 3449
Kew W. et al. 2018, Anal. Chem., 90, 11265
Kruve A. et al. 2013, J. Mass Spectrom., 48, 695
Lababidi S., Schrader W. 2014, Rapid Commun. Mass Spectrom., 28, 1345
Liigand J., Laaniste A., Kruve A. 2017, J. Am. Soc. Mass. Spectrom., 28, 461
Marshall A. G., Hendrickson C. L., Jackson G. S. 1998, Mass Spectrom. Rev., 17, 1
Materese C. K. et al. 2015, ApJ, 812, 150
McClure M. K. et al. 2023, Nat. Astron., 7, 431
McEwen C. N., Larsen B. S. 2009, J. Am. Soc. Mass. Spectrom., 20, 1518
Meierhenrich U. J. et al. 2005, Chem. Eur. J., 11, 4895
Meinert C. et al. 2016, Science, 352, 208
Modica P. et al. 2014, ApJ, 788, 79
Modica P. et al. 2018, ApJ, 865, 41
Mojarro A. et al. 2025, Proc. Natl. Acad. Sci., 122, e2512461122
Moore M. H., Hudson R. L., Gerakines P. A. 2001, Spectrochim. Acta A, 57, 843
Muñoz Caro G. M. et al. 2002, Nature, 416, 403
Muñoz Caro G. M. et al. 2004, A&A, 413, 209
Muñoz Caro G. M. et al. 2014, A&A, 566, A93
Muñoz Caro G. M., Schutte W. A. 2003, A&A, 412, 121
Naraoka H. et al. 2023, Science, 379, eabn9033
Nguyen A. N. et al. 2025, Nat. Astron., 9, 1812
Nikolaev E. N., Kostyukevich Y. I., Vladimirov G. N. 2016, Mass Spectrom. Rev., 35, 219
Nuevo M. et al. 2007, Adv. Space Res., 40, 1628
Nuevo M., Cooper G., Sandford S. A. 2018, Nat. Commun., 9, 5276
Oba Y. et al. 2019, Nat. Commun., 10, 4413
Oba Y. et al. 2020, Nat. Commun., 11, 6243
Öberg K. I. 2016, Chem. Rev., 116, 9631
Ohno T. et al. 2010, Environ. Sci. Technol., 44, 8594
Omari I. et al. 2019, J. Am. Soc. Mass. Spectrom., 30, 1750
Robb D. B., Covey T. R., Bruins A. P. 2000, Anal. Chem., 72, 3653
Rocha W. R. M. et al. 2024, A&A, 683, A124
Rodríguez-Lazcano Y. et al. 2014, Phys. Chem. Chem. Phys., 16, 3371
Rohner T. C., Lion N., Girault H. H. 2004, Phys. Chem. Chem. Phys., 6, 3056
Ruf A. et al. 2017, Proc. Natl. Acad. Sci., 114, 2819
Ruf A. et al. 2019, ApJ, 887, L31
Ruf A., Danger G. 2022, Anal. Chem., 94, 14135
Sandford S. A. et al. 2025, Nat. Astron., 9, 1803
Schmitt-Kopplin P. et al. 2010, Proc. Natl. Acad. Sci., 107, 2763
Schmitt-Kopplin P. et al. 2023, Nat. Commun., 14, 6525
Shen C. J. et al. 2004, A&A, 415, 203
Sleighter R. L., Hatcher P. G. 2007, J. Mass Spectrom., 42, 559
Song L. et al. 2007, J. Am. Soc. Mass. Spectrom., 18, 1789
Song L. et al. 2009, J. Am. Soc. Mass. Spectrom., 20, 42
Strazzulla G., Castorina A. C., Palumbo M. E. 1995, Planet. Space Sci., 43, 1247
Takano Y. et al. 2004, Appl. Phys. Lett., 84, 1410
Tenelanda-Osorio L. I. et al. 2022, MNRAS, 515, 5009

Theulé P. et al. 2013, Adv. Space Res., 52, 1567
Urso R. G. et al. 2020, A&A, 644, A115
Urso R. G. et al. 2022, A&A, 668, A169
Van Dishoeck E. F., Jonkheid B., Van Hemert M. C. 2006, Faraday Discuss., 133, 231
Vinogradoff V. et al. 2011, A&A, 530, A128
Wilm M. 2011, Mol. Cell. Proteomics, 10, M111.009407
Wollrab E. et al. 2016, Orig. Life Evol. Biosph., 46, 149
Wooden D. H., Charnley S. B., Ehrenfreund P. 2004, Comets II, University of Arizona Press, 33
Yassine M. M. et al. 2014, Rapid Commun. Mass Spectrom., 28, 2445

## AUTHOR CONTRIBUTION

LH, AD, and GD conceived the study. LH, JH, VC, FA, and G. developed the methodology and performed the investigation. LH, AR, and GD carried out the formal analysis, software implementation, and visualization. LH prepared the original draft of the manuscript, while GD, AD, JH, VC, FA, and AR contributed to the review and editing. JH and PSK provided resources by sharing previously acquired data that were reprocessed by LH, GD, and AD supervised the project.

## SUPPORTING INFORMATION

Supplementary data are available at *MNRAS* online.

Please note: Oxford University Press is not responsible for the content or functionality of any supporting materials supplied by the authors. Any queries (other than missing material) should be directed to the corresponding author for the article.

This paper has been typeset from a Microsoft Word file prepared by the author.